1. Introduction for AY 219

The periodic table of the elements – absolutely key for this class. There is an interactive on-line periodic table of the elements at Los Alamos Ntl Lab's we site, http://periodic.lanl.gov/default.htm. You can click on an element and get some useful information about it. The Commission on Isotopic Abundances and Atomic Weights (part of the IAU of Pure and Applied Chemistry) also has a useful web site. Some properties of elements depend on number of electrons in the outermost shell. When this is full (closed) get noble gases (He, Ne, Ar) which do not react easily. Families of elements with a specific number of electrons in the outermost shell, or number missing to fill the outermost shell, such as the alkali metals with one free electron (Li, Na, K, ...). These are highly reactive and are never found in elemental form in nature, just in compounds. The halogens (F, Cl, Br, ...) are missing one electron to form a closed shell and hence are also very reactive.

There is no element with a stable isotope heavier than Bi (atomic number 83).

The Berkeley Laboratory Isotopes Project has an interactive web page (http:/ie.lbl.gov/education/isotopes.htm) giving information on the isotopes, both stable and unstable, of each element.

Note that there are **no** stable isotopes of atomic mass 5 and 8. This will be important in working out nuclear reaction chains.

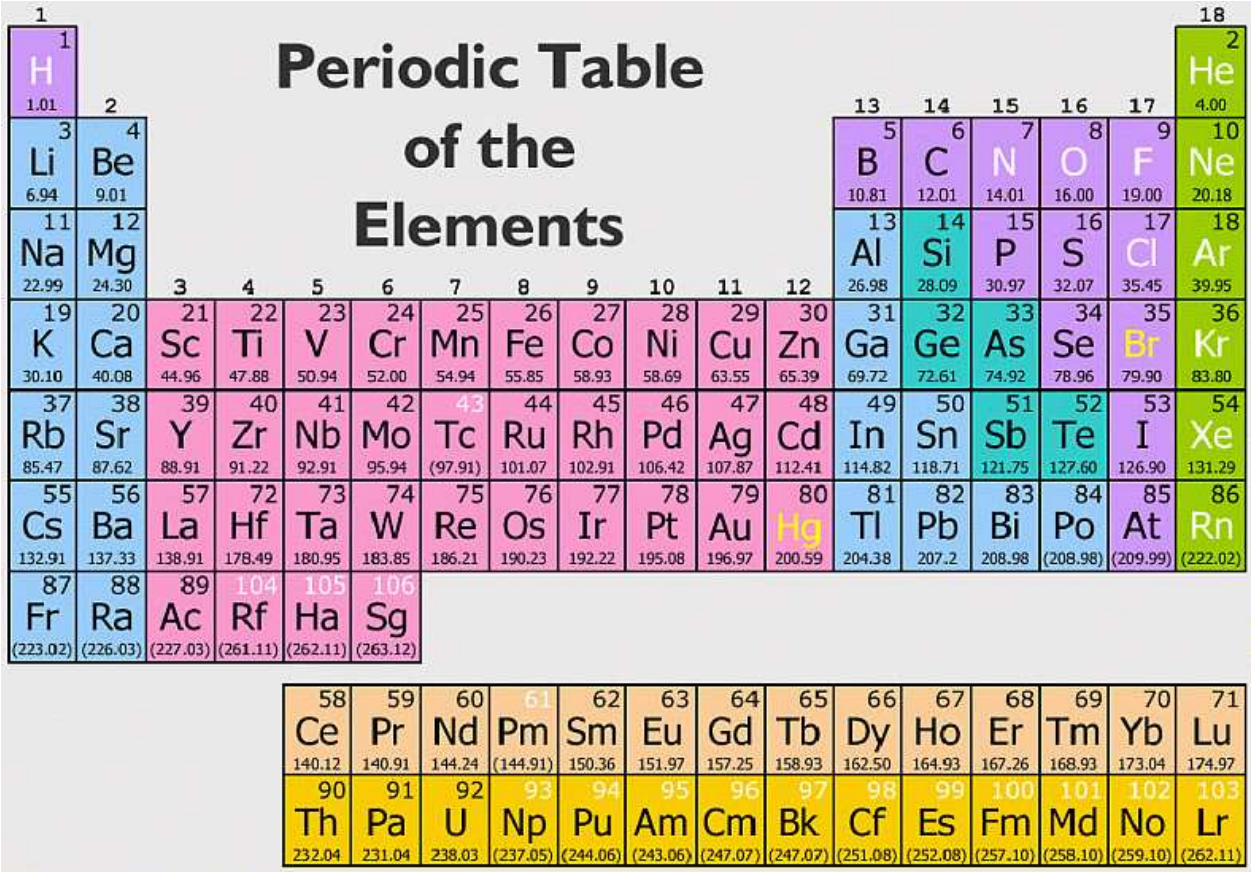

Fig. 1.— The periodic table of the elements.

1.1. Solar System Abundances

The Solar abundances can be determined from analysis of the photospheric line spectrum – that is the standard way. Solar interior abundances have already been slightly affected by ongoing nuclear reactions, so the photospheric abundance are the standard used and are taken as representative of the ISM at the time that the Sun was formed. Note that abundances in the present day Sun may not be identical to those of the ISM when the Sun was formed due to possible settling of He and other heavy elements. The difference should be small, but we need models for guidance, the magnitude of this depends on details of convective zones.

Recent critical compilations and analysis for the Solar abundances can be found in Lodders, Palme & Gail (2009, New Series, A&A, arXiv:0901.1149) and also in Asplund, Grevesse, Sauval & Scott (2009, ARA&A, 47, 481). The latter does a careful reanalysis of the solar spectrum, attempting to include some previously neglected detailed effects (non-LTE, 3D models for convection rather than 1D plane parallel layers). The results of Asplund et al (2009) have given rise to a lot of controversy, because they lower the CNO abundances enough to reduce Z for the Sun. (Z is the fraction by mass of elements heavier than H and He, and is dominated by the most abundance elements, which are C N O Ne Mg Si and Fe.) This decrease in Z destroys the good agreement between observed and predicted helioseismology (the study of the frequencies of resonant oscillation of the Sun, which can be predicted very accurately from detailed solar models, and measured very accurately from campaigns with networks of small telescopes around the world), which in the past was regarded as a triumph of our understanding of the Sun. The previous standard set of solar abundances were those of Anders & Grevesse (1989, Geochim. Cosmochim. Acta, 53, 197). The differences for most elements between these various compilations is small, less than 0.08 dex (a factor of 1.2), except for the CNO elements and others with

very few if any detectable photospheric absorption lines.

Solar wind abundances can be measured by satellites. See the discussion of ACE later in this document for some of the limitations of such measurements.

The meteoritic abundances are much more accurately known than the photospheric ones (after all they can be measured in a lab on Earth in objects with masses of kg), but volatile material (any component initially a gas) is depleted in meteorites (i.e. H, He etc). However, ignoring the volatile elements, the agreement between current photospheric and meteoritic abundances of elements is quite good.

The crust of the Earth consists mostly of silica (SiO_2), alumina (Al_2O_3), lime (CaO), magnesia (MgO), iron oxide (FeO) and other minerals including water and CO_2 in small amounts. It is about 60% by weight oxygen. The core of the Earth is believed, on the basis of the behavior of seismic waves, to be liquid, with a solid inner core composed primarily of Fe, with smaller amounts of Ni and other trace elements.

Thus, unlike the Sun, the Earth is highly differentiated, with different spatial regions having very different chemical comopositions.

The Earth's atmosphere is also quite dissimilar to the Sun, with a large deficit of H and He, which presumably escaped from the Earth's gravitational field. The dominant constituent is N_2, with O_2 a strong second, and everything else being trace gases. Water is only a few percent of the atmosphere even near the surface of the Earth.

Key points to note regarding the Solar abundances are:

1. Strong and sustained drop from lighter to heavier elements with an enormous range of 10^{12} between H and Th or U (both of which have no stable isotops) or Ta.

2. strong odd/even effect with even atomic number elements have significantly higher Solar

abundances than their odd number neighbors.

3. strong odd/even effects for isotopes of the same element. The even atomic weight isotopes have higher abundances than the adjacent odd ones.

4. Peaks at Fe, Ba, Pb.

5. The Solar photospheric and meteoritic abundances agree well for non-volatile species.

6. The Sun has a chemical inventory similar to that of field stars of its same overall metallicity. It is not anomalous.

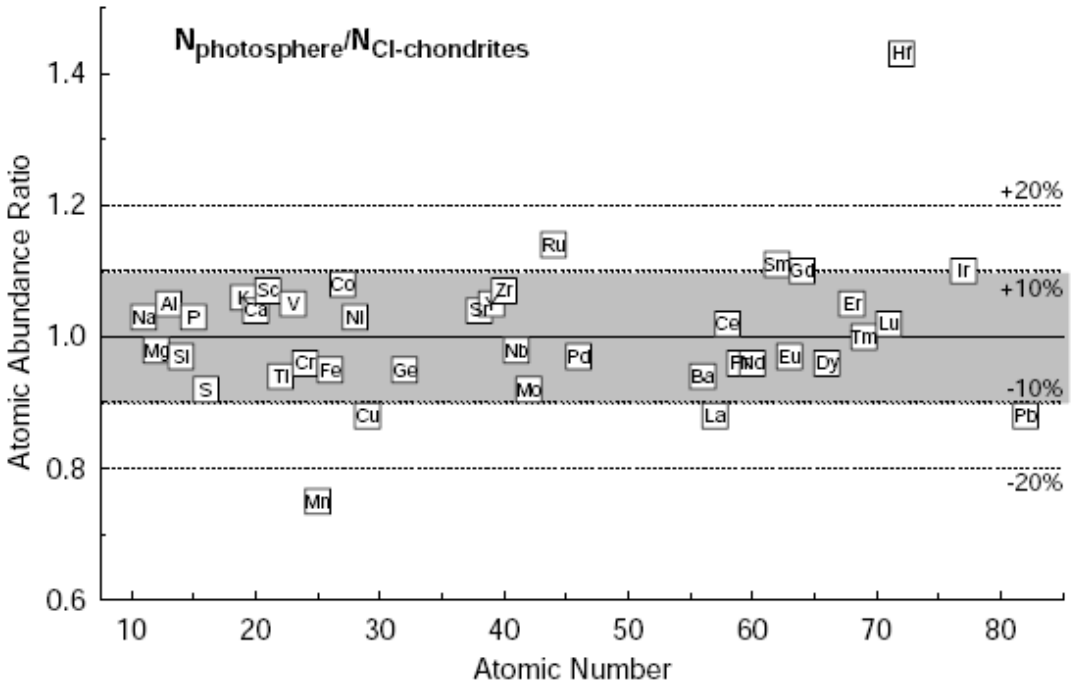

Fig. 4. Comparison of photospheric and CI-chondrite abundances, excluding highly volatile elements. Only elements with uncertainties below ~ 25% (<0.10 dex) in the photospheric abundance determinations are shown. The grey-shaded area is for elements that agree within ±10%; the range for 20% agreement is shown by the other dotted lines. Hafnium and Mn are well determined in meteorites and in the Sun, but differ by more than 30 %. Lithium and Be would also qualify for inclusion in this diagram but are not included. Lithiumis by a factor of more than 100 higher in meteorites, because it is destroyed in the interior of the Sun by nuclear reactions. Beryllium only differs 15, suggesting less or no destruction by nuclear reactions.

Fig. 2.— The ratio of Solar photospheric/meteoritic abundances for non-volatile elements for chondrites (stony meteorites that have never been modified due to melting or any other type of differentian within the parent body). Fig. 4 of Lodders, Palme & Gail, 2009, New Series, A&A. See arXiv:0901.1149

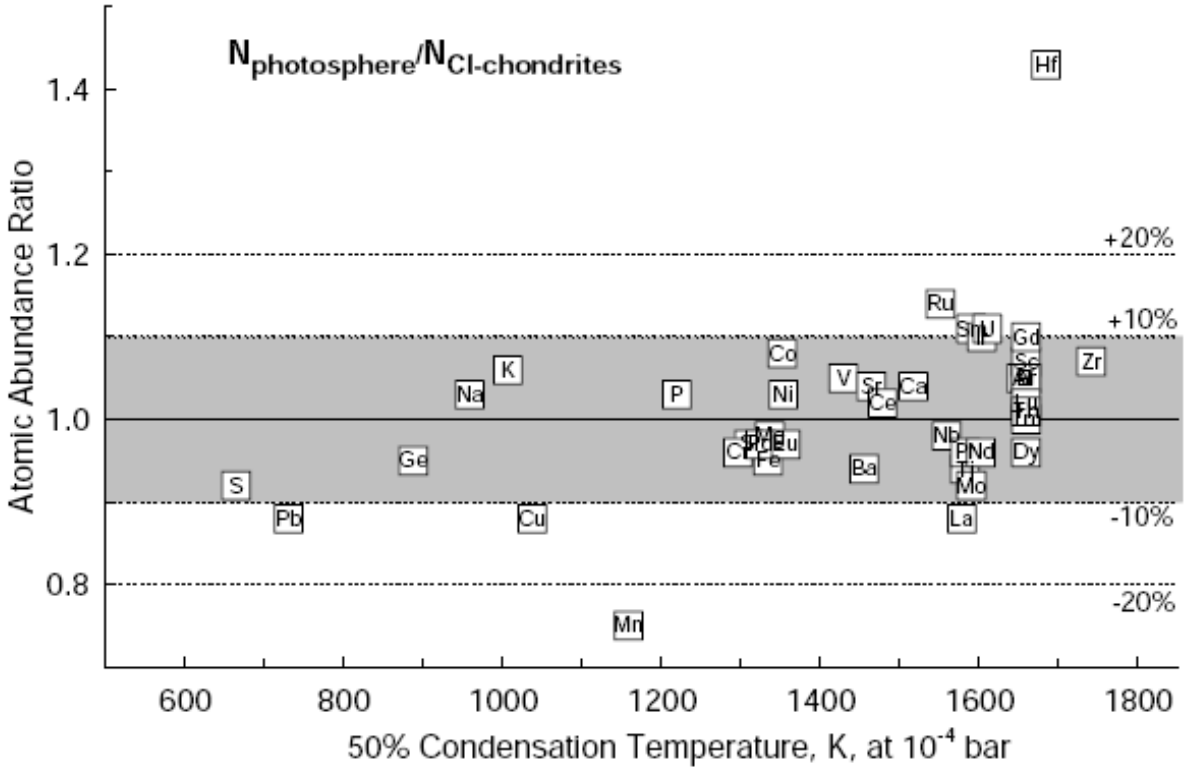

Fig. 5. Same as Fig. 4, but abundance ratios are plotted as function of 50% condensation temperatures. The agreement between solar and meteoritic abundances is independent of the volatility of the elements.

Fig. 3.— The ratio of Solar photospheric/meteoritic (chondrites) abundances for non-volatile elements as a function of condensation temperature. Fig. 5 of Lodders, Palme & Gail, 2009.

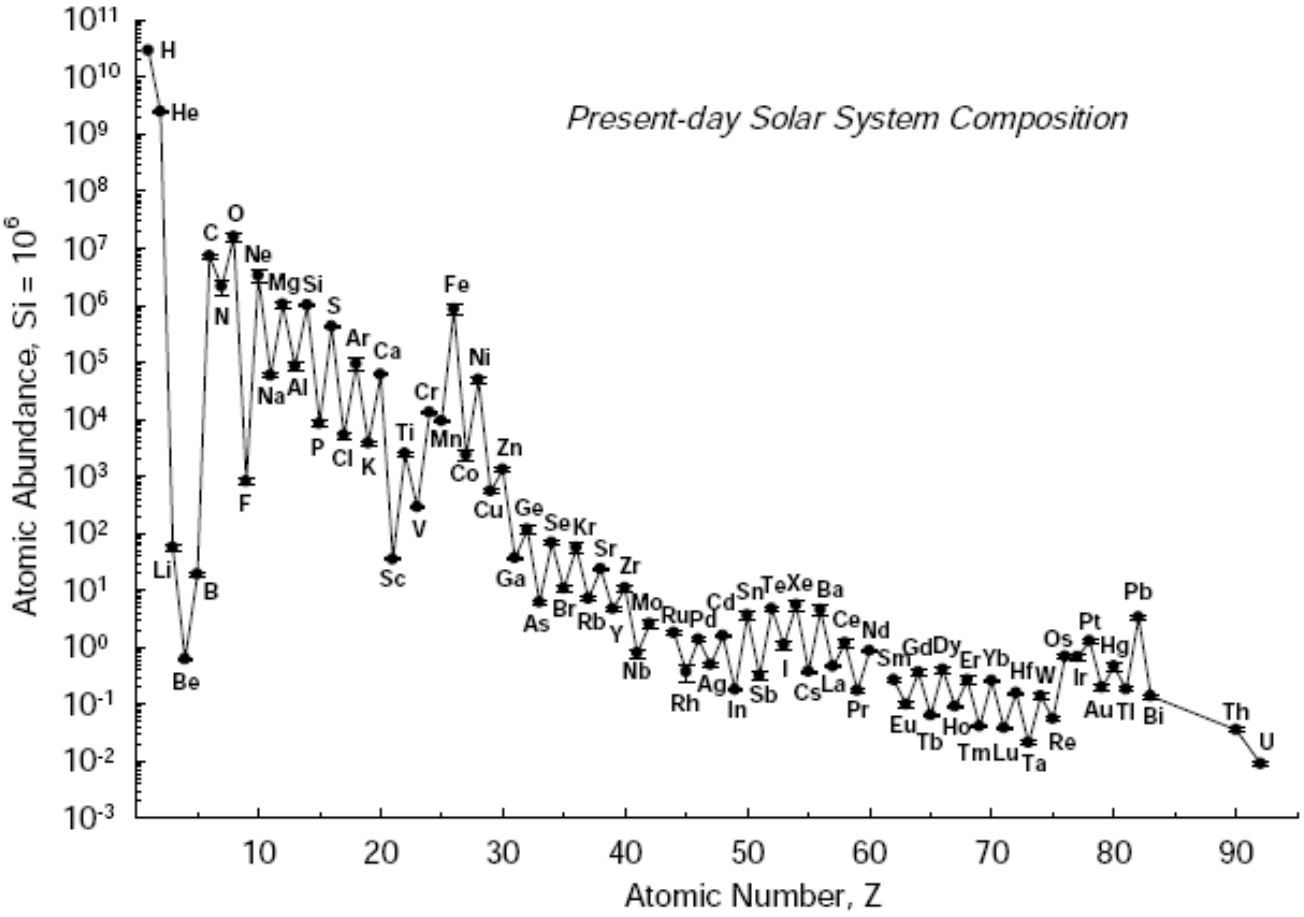

Fig. 6. Elemental present-day solar system abundances as function of atomic number normalized to 10^6 Si atoms. The stability of ^{56}Fe and the higher stability of elements with even atomic numbers are clearly visible.

Fig. 4.— The present day Solar abundances of the elements. Fig. 6 of Lodders, Palme & Gail, 2009.

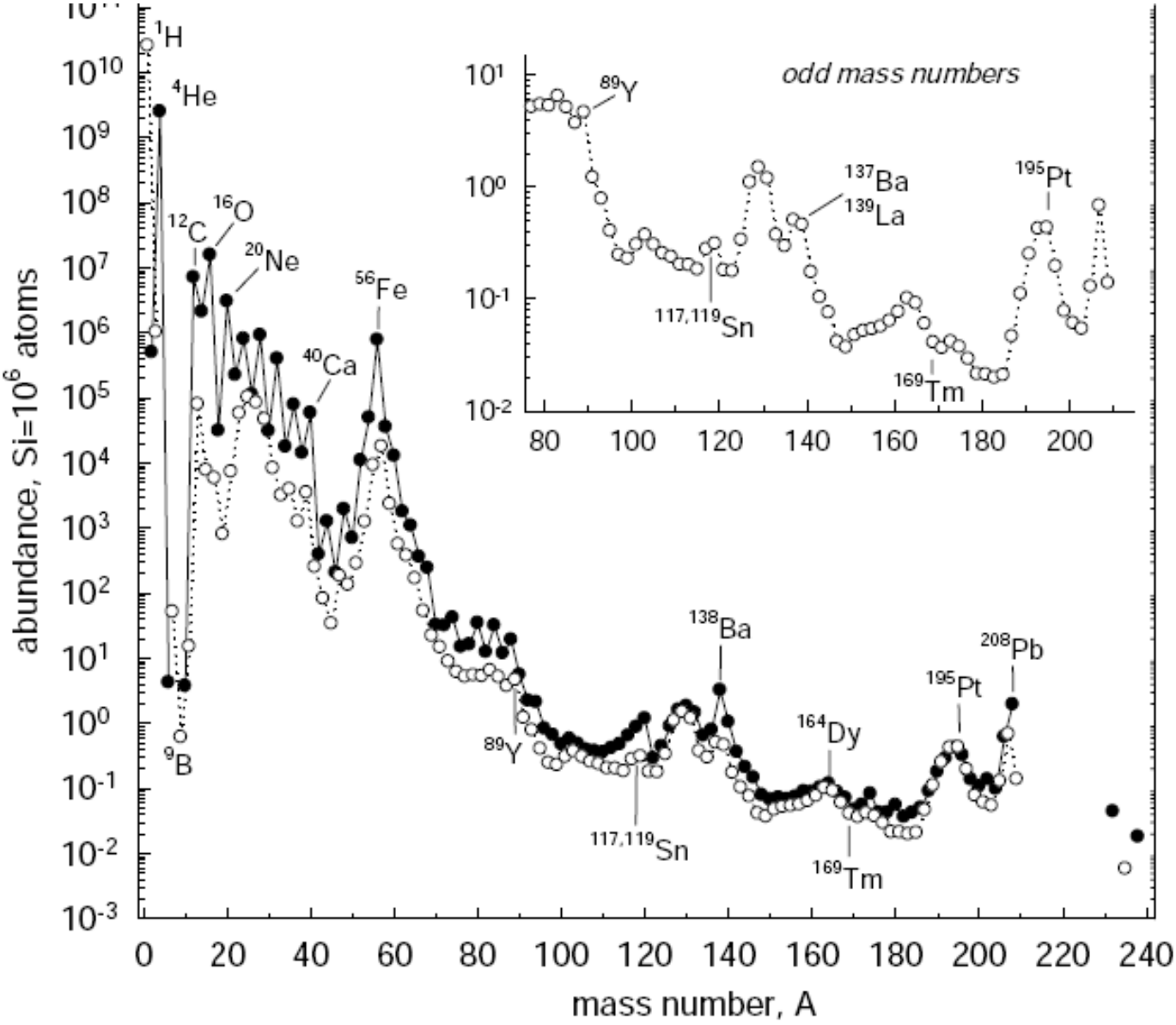

Fig. 7. Nuclide abundances plotted versus mass number. Open symbols are for odd mass numbers and full symbols are for even ones. The odd numbered nuclides form an approximately smooth curve (insert in Figure). Suess [47S] attached significance to this smoothness and suggested that elements with poorly known abundances may be found by extrapolation. The abundance curve has, however, kinks (e.g. at Sn) inconsistent with smooth abundances.

Fig. 5.— The present day Solar abundances of the isotopes of each element. Fig. 7 of Lodders, Palme & Gail, 2009.

Table 8. Present-day solar composition (mass %)

	this work	[05A1,07G]	[98G]
H (=X)	73.90	73.92	73.47
He (=Y)	24.69	24.86	24.83
O	0.63	0.54	0.79
C	0.22	0.22	0.29
Ne	0.17	0.10	0.18
Fe	0.12	0.12	0.13
N	0.07	0.06	0.08
Si	0.07	0.07	0.07
Mg	0.06	0.06	0.07
S	0.03	0.03	0.05
all other elements	0.04	0.02	0.04
total heavy elements (=Z)	1.41	1.22	1.69

Fig. 6.— The present day Solar fractions by mass of the elements. Table 8 of Lodders, Palme & Gail, 2009.

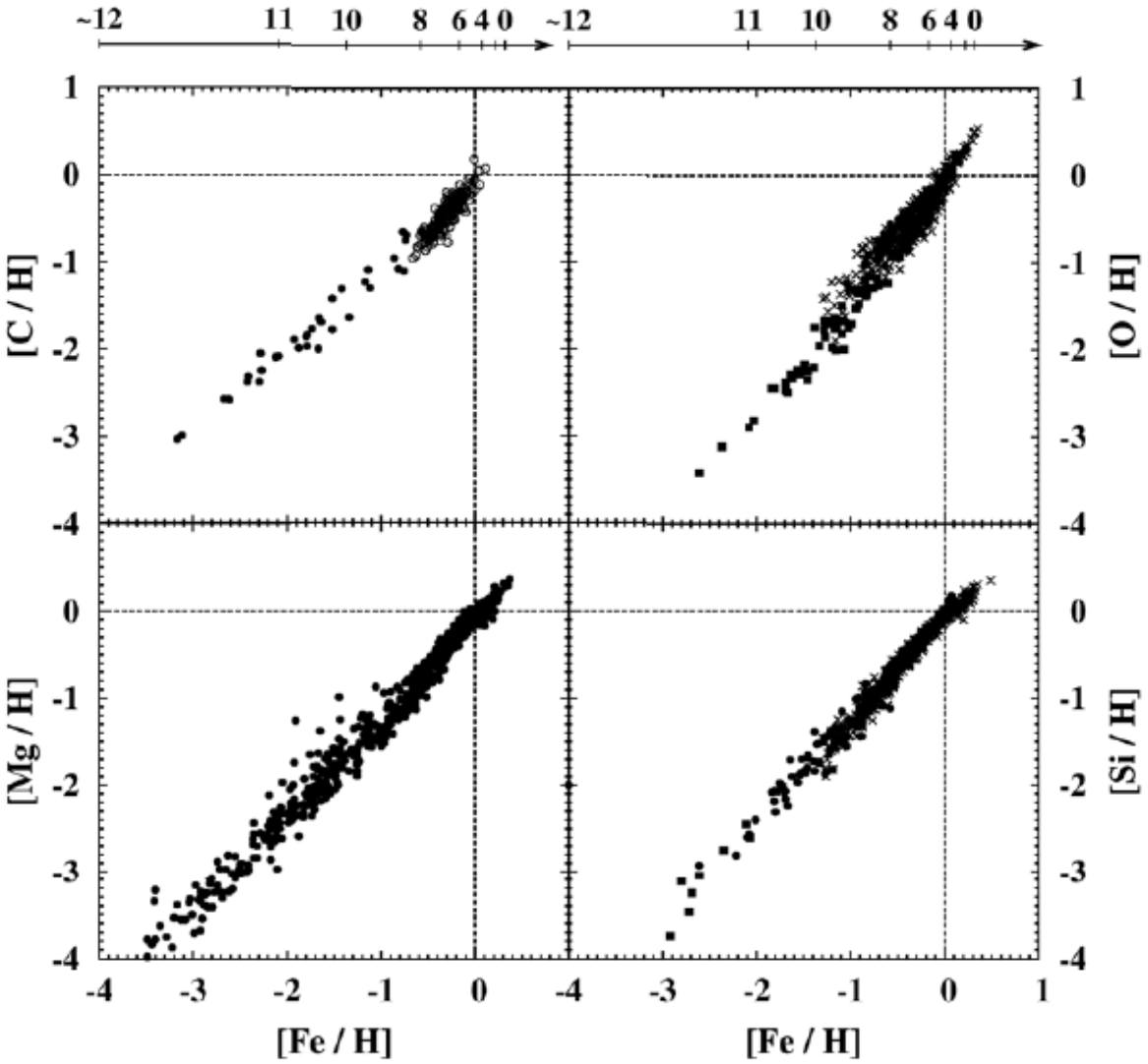

Fig. 8. Evolution of element abundances relative to H in the solar neighbourhood of some of the most abundant metals derived from main sequence G-stars. The range of metallicities -4 < [Fe/H] < 0.3 corresponds to stellar ages from ~12 Ga ([Fe/H] ~ -4) to less than 1 Ga ([Fe/H] ~0.2). The dashed lines correspond to solar abundances, i.e., abundances of the ISM 4.6 Ga ago. Solar abundances are within the range of observed abundances of other G-stars with same metallicity. Data sources: [04A2, 03R] for C, [00C, 05S2] for O, [04V] for Mg, [88G, 91G, 03G, 05S2] for Si.

Fig. 7.— How typical is the Sun ? Fig. 8 of Lodders, Palme & Gail, 2009.

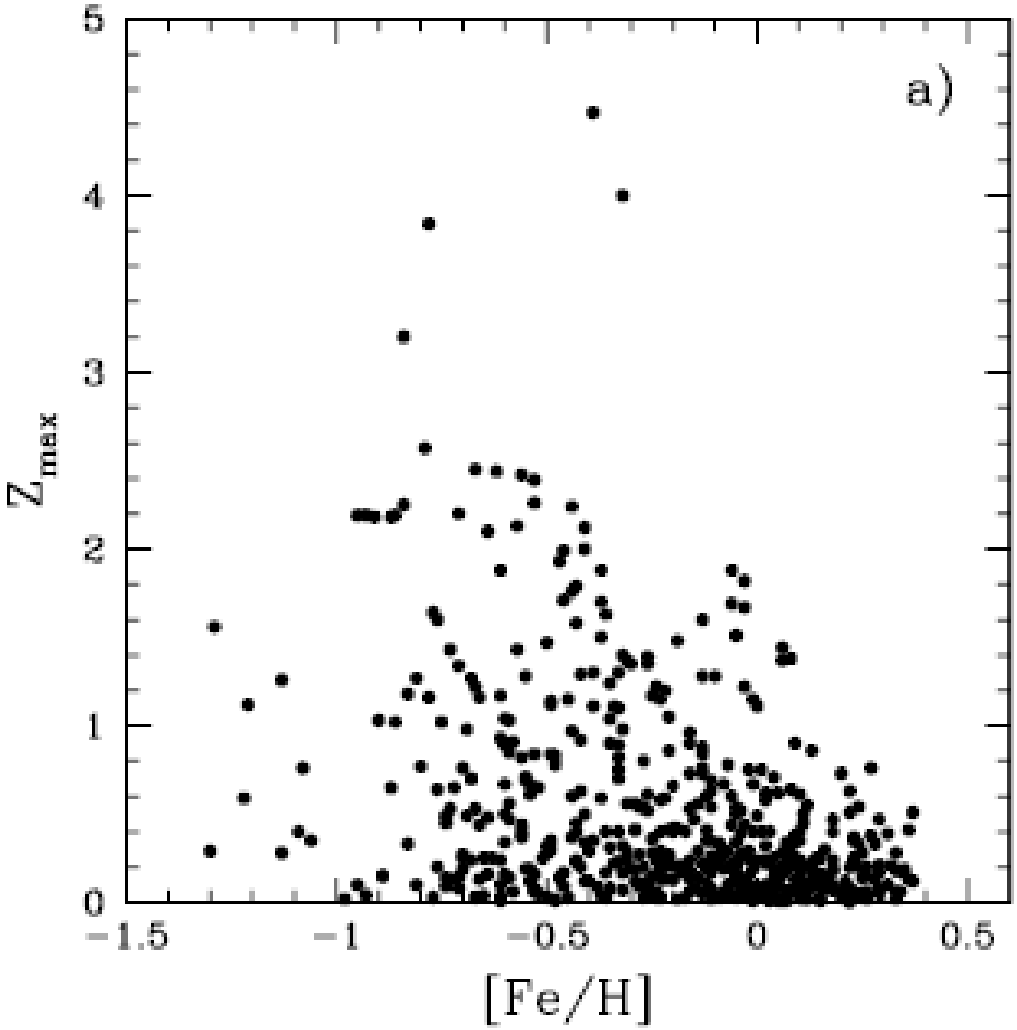

Fig. 8.— How typical is the Sun ? Note that by definition [Fe/H] is 0.0 for the Sun. Fig. 4 from Feltzing & Bensby, conference contribution, 2009 (see arXiv:0811.1777).

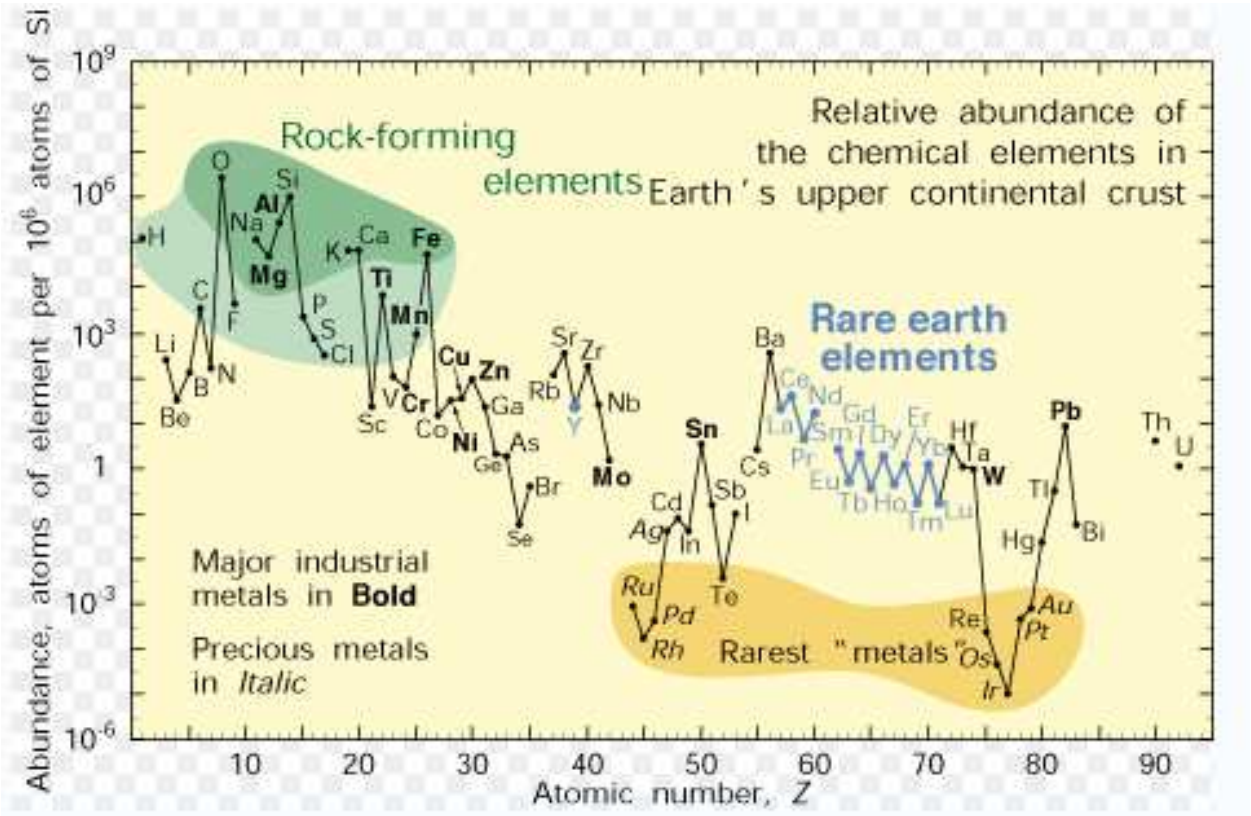

Fig. 9.— The composition of the Earth's continental crust.

1.2. Pre-Solar Grains

Material from the gas phase can condense onto grains in the low temperature outer atmospheres of cool stars. These grains contain refractory material which has a condensation temperature higher than that characteristic of this part of the stellar atmosphere. The dust grains are driven away from the star by stellar winds, contain refractory material only, gas is lost, subsequently swept up in the ISM, and may subsequently become embedded in asteroids. When asteroids get too close to the Sun, they break apart, and the pieces become meteorites if they impact the Earth.

Non-mixed, non-homogenized "primitive meteorites" such as chondrites, which are rare, are the ones of interest. If you break up the solid meteorite and dissolve the pieces in various chemicals, you can find pre-solar grains. They can be recognized via their unusual isotopic ratios. Since these can be measured in a lab, the isotopic ratios for a particular element in each small pre-solar grain can be determined to an accuracy of 1 part in 10^4 or better.

These grains lack the homogeneity and smoothing of the current ISM and solar material, which contain ejecta from many generations of SN, AGB stars, etc. There are several different types of pre-solar grains, some appear to be from SN, some from dust grains formed in outer envelopes of cool stars. These grains are typically very small, only about a micron in size. To study them you need a very good clean room, and sophisticated lab equipment.

They can also be studied by spacecraft with suitable high precision mass spectrometers that are in the outer solar system, i.e. Galileo and Ulysses. The limited equipment on such satellites means that one can only measure the distribution of mass of grains within the local ISM; there is no satellite information on elemental abundances. Charged grains and very small grains may not penetrate the heliosphere to get close enough to the Sun to be

picked up by spacecraft. (Recall that the Solar wind is pushing material outward from the Sun, at least until the heliopause at the outed edge of the Solar system, so a minimum energy is required for an incoming particle to get far enough inside to reach the Earth's orbit.)

The detailed isotopic composition of the various pre-solar grains is a fabulous tool for nucleosynthesis, and hopefully will be chosen as a topic for a student presentation later in the class. I ran across three recent review articles, Lodders & Amari (2005, Chemie der Erde, 65, 93) which is in Astro-ph, E. Zinner (2007, Geochem. Cosmochim Acta, 71, 4786), and P. Hoppe (2008, Space Science Rev, 138, 43).

Because very small fractional changes in isotopic composition can be measured in the lab, papers on pre-solar grains often use the parameter δ to describe the isotopic or atomic over or underabundances with respect to Solar composition.

$$\delta^i N \;=\; 1000 \;\times\; [\frac{(^iN/^jN)(sample)}{(^iN/^jN)(standard)} \;-1].$$

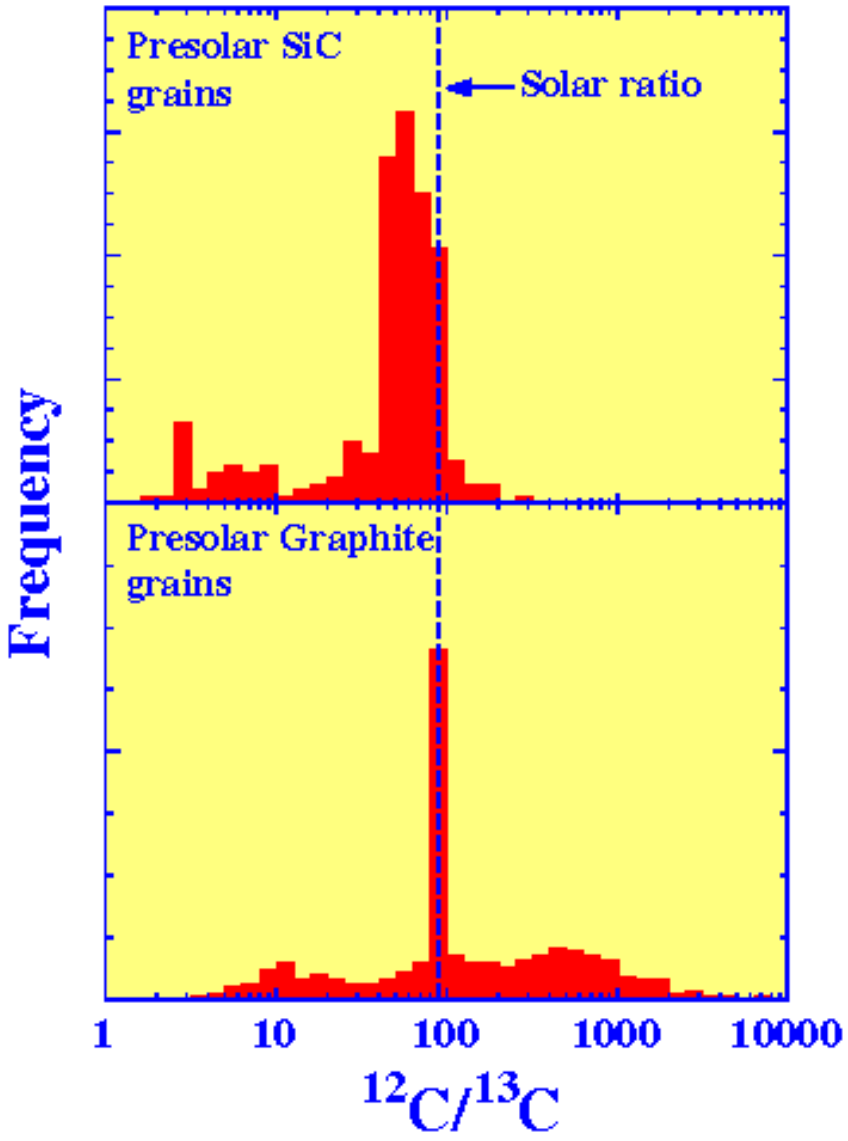

Fig. 10.— The C isotope ratios in two different types of pre-solar grains. The Solar ratio of $^{12}C/^{13}C$ is 89. The range among the pre-solar grains is 1/20 to 100 times to Solar ratio. This figure is from www.dtm.ciw.edu/users/nittler/psg_main.html; you might want to look at the pictures of pre-solar grains on this website.

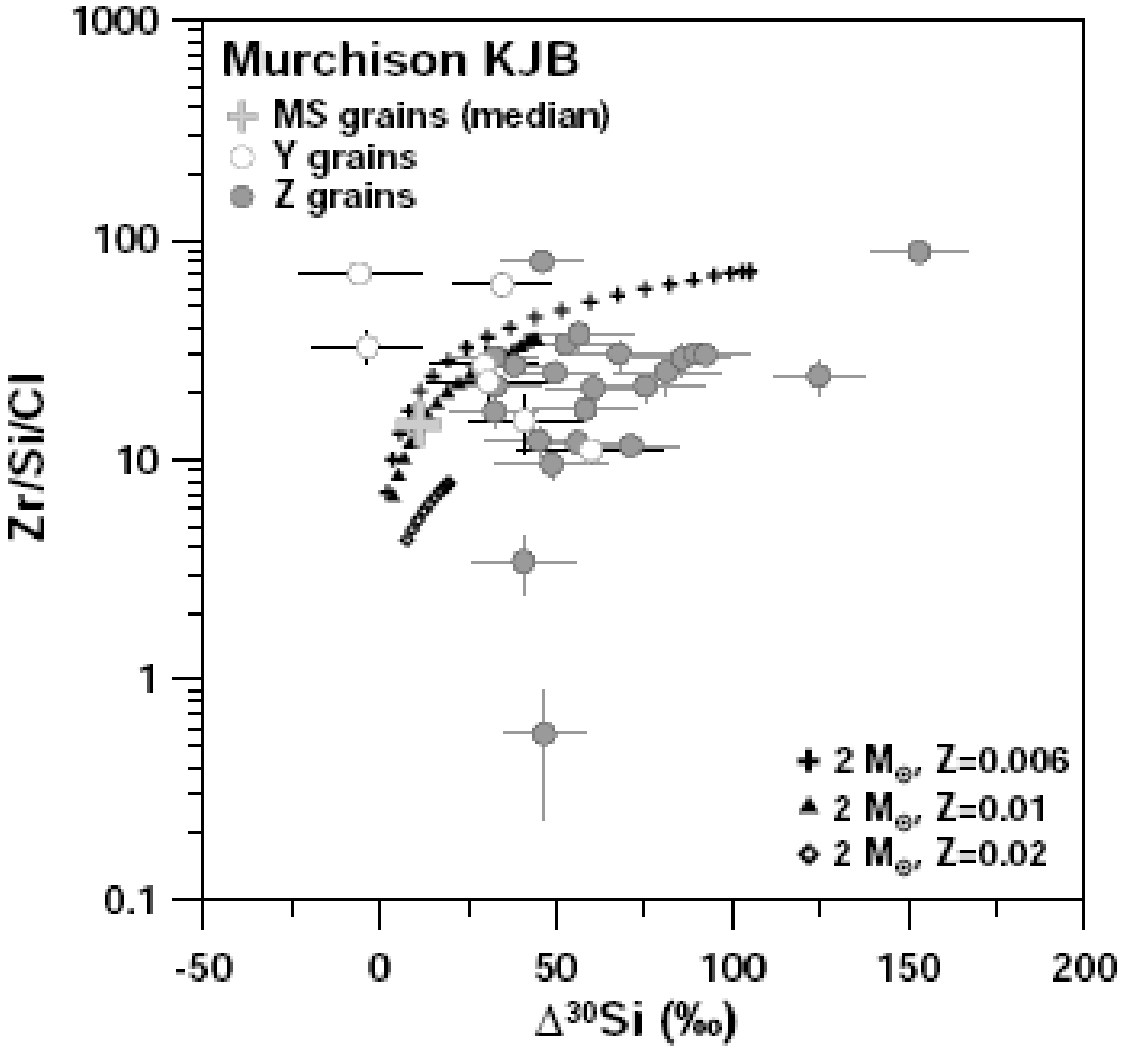

Figure 4 Zr/Si ratios normalized to solar (CI) in Y and Z grains as a function of Δ^{30}Si (cf. Fig. 3). Errors are 1σ. Median values for mainstream (MS) grains and model predictions for 2 $M_\odot$ AGB stars with three different metallicities, standard ^{13}C pocket, and C/O > 1 are shown for comparison.

Fig. 11.— The ratio of the abundances of the heavy neutron capture element Zr to that of Silicon in pre-solar grains. From Hoppe, Leitner, Vollmer et al, 2009, PASA, 26, 284

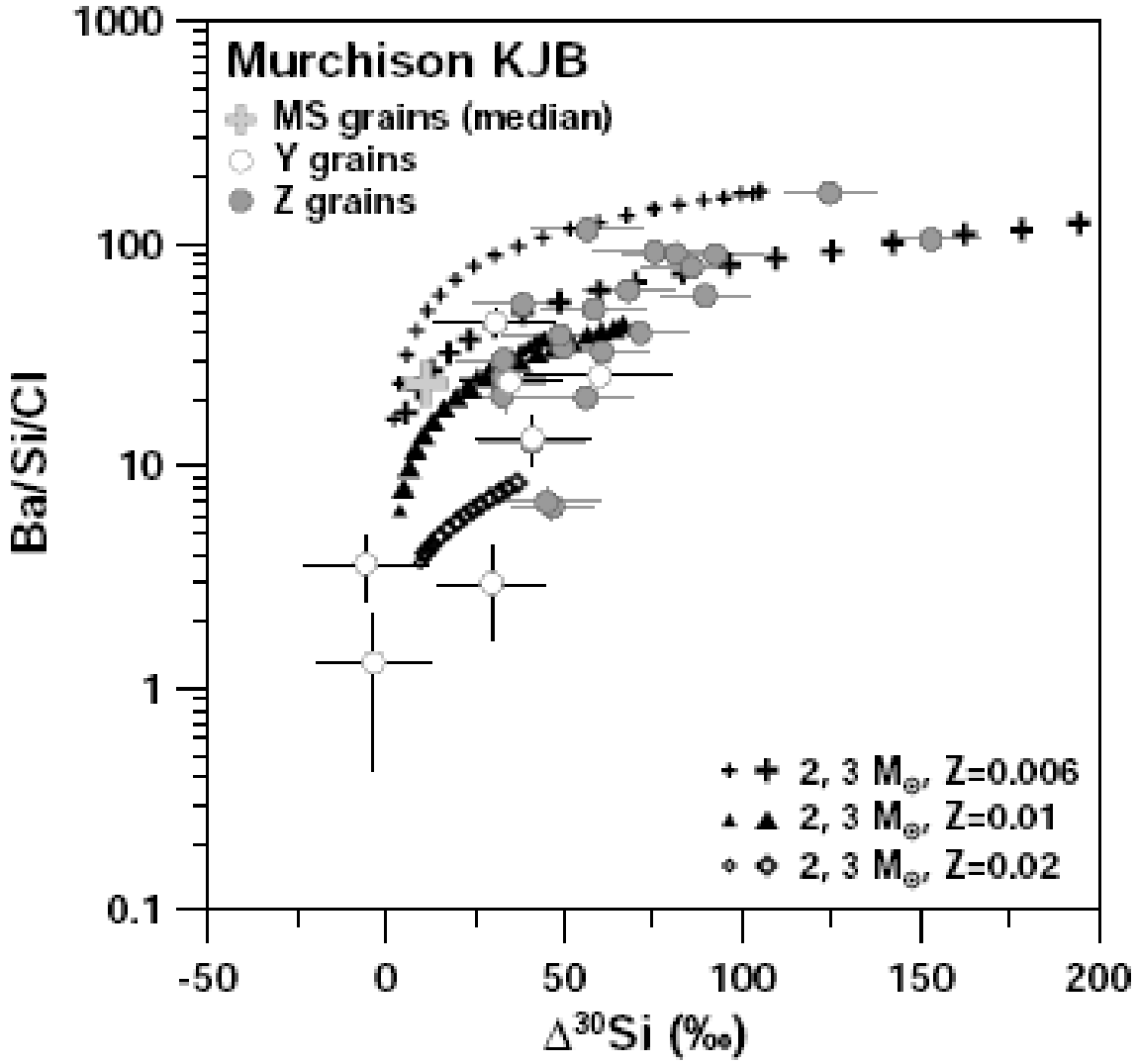

Figure 5 Ba/Si ratios normalized to solar (CI) in Y and Z grains as a function of Δ^{30}Si (cf. Fig. 3). Errors are 1σ. Medain values for mainstream (MS) grains and model predictions for 2 and 3 $M_\odot$ AGB stars with three different metallicities, standard ^{13}C pocket, and C/O > 1 are shown for comparison.

Fig. 12.— Same as the previous figure for the even heavier neutron capture element Ba. From Hoppe, Leitner, Vollmer et al, 2009, PASA, 26, 284

Table 3. Currently known presolar minerals

Mineral	Characteristic size	Possible stellar source [a]	Discovery papers
Diamond	2 nm	AGB?, SN?	Lewis et al. 1987
SiC	0.1 – 20 μm	AGB, SN, novae	Bernatowicz et al. 1987, Tang and Anders 1988
graphite	1 – 20 μm	AGB, SN	Amari et al. 1990
carbides in graphite	10 – 200 nm	AGB, SN	Bernatowicz et al. 1991, 1996,
metal grains in graphite	10 – 20 nm	SN	Croat et al. 2003, 2004
Si_3N_4	0.3 – 1 μm	AGB?, SN	Nittler et al. 1995
corundum (Al_2O_3)	0.2 – 3 μm	RGB, AGB, SN?	Hutcheon et al. 1994, Nittler et al. 1994
spinel ($MgAl_2O_4$)	0.2 – 3 μm	RGB, AGB, SN?	Nittler et al. 1997, Choi et al. 1998
hibonite ($CaAl_{12}O_{19}$)	0.2 – 3 μm	RGB, AGB, SN?	Choi et al. 1999
TiO_2			Nittler and Alexander 1999
silicates (olivine, pyroxene)	0.1 – 0.3 μm	RGB, AGB, SN?	Messenger et al. 2003 (in IDPs), Nguyen and Zinner 2004 (in chondrites)

Notes. [a] AGB: asymptotic giant branch stars. RGB: red giant branch stars. SN: supernovae. A "?" indicates not known/uncertain.

Fig. 13.— Table 3 of Lodders & Amari (2005, Chemie der Erde, 65, 93).

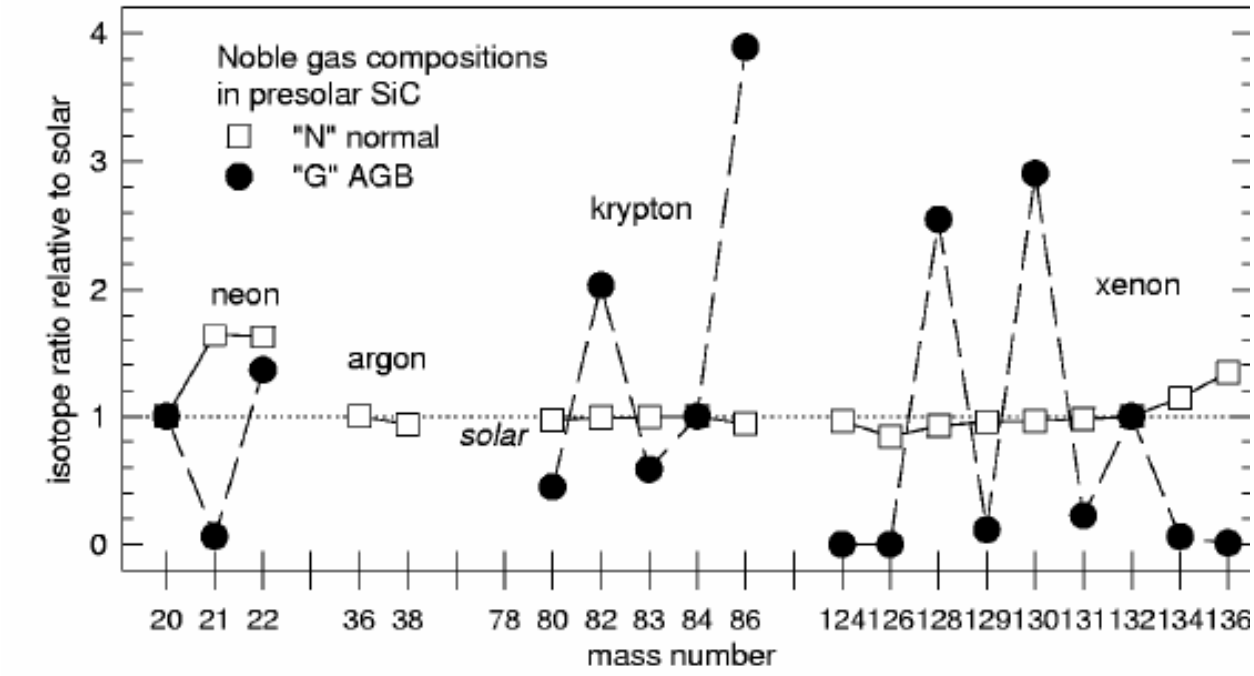

Fig. 5. Noble gas components in aggregates of SiC grains (Lewis et al. 1990, 1994, Ott 200 normalized to solar isotopic composition (Wieler 2002). Isotope ratios are further normalized t ^{20}Ne, ^{36}Ar, ^{84}Kr, and ^{132}Xe, respectively. The dotted line shows solar composition.

Fig. 14.— Fig. 5 of Lodders & Amari (2005, Chemie der Erde, 65, 93).

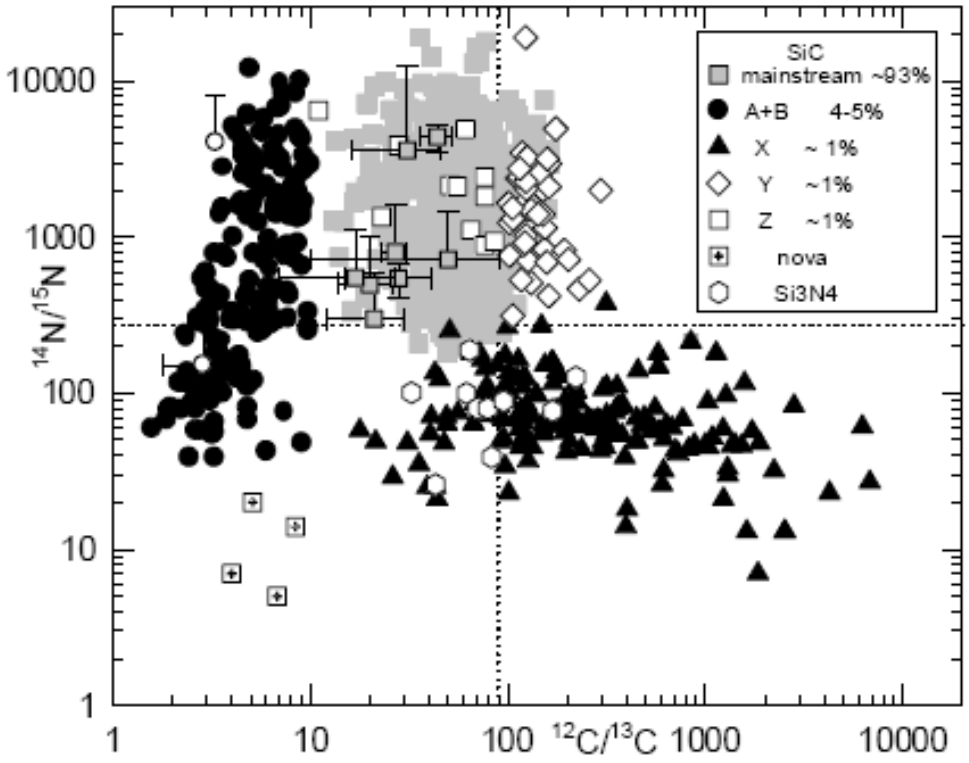

Fig. 6. SiC grains fall into different populations based on their C- and N-isotope ratios (Alexander 1993, Amari et al. 2001a-c, Hoppe et al. 1994, 1997,2000, Huss et al. 1997, Lin et al. 2002, Nittler et al. 1995). For comparison, stellar data are plotted with error bars and their N-isotopic ratios are typically lower limits (Wannier et al. 1991, Querci and Querci 1970, Olsen and Richter 1979). The dotted lines indicate solar isotope ratios.

Fig. 15.— Fig. 6 of Lodders & Amari (2005, Chemie der Erde, 65, 93).

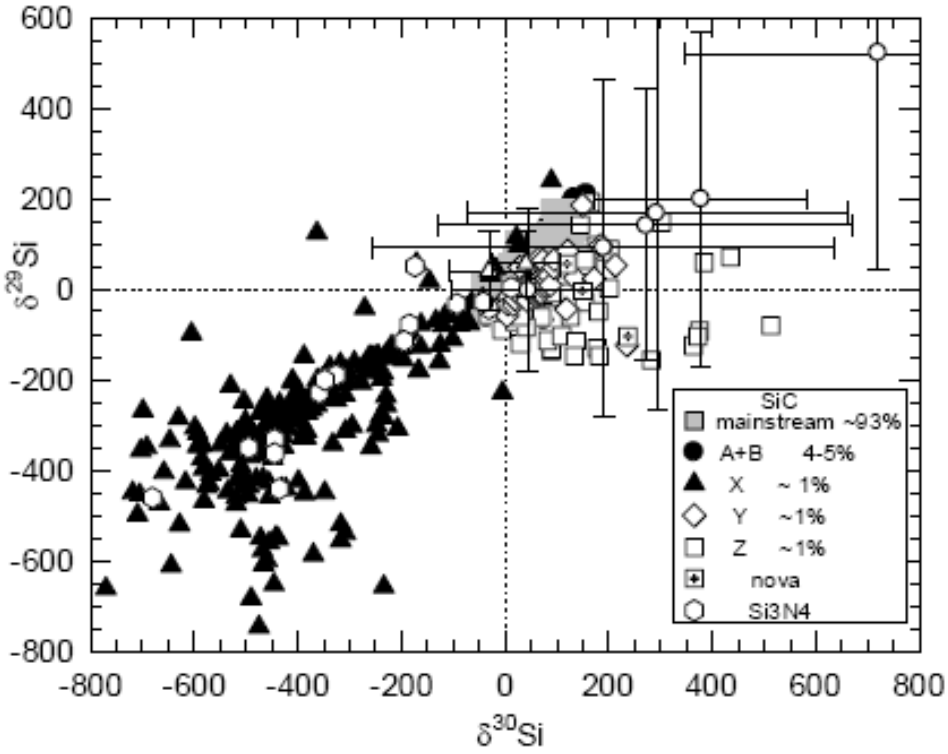

Fig. 7. The Si-isotopes for presolar SiC grains (references as in Fig. 6) and stars (symbols with error bars) are given in the δ–notation which describes the deviation of an isotope ratio ($^iN/^jN$) of a sample from the (terrestrial) standard ratio in per-mil: δ^iN (‰) = $[(^iN/^jN)_{sample}/(^iN/^jN)_{standard} - 1] \times 1000$. The grains fall into distinct populations. The triangles show two determinations for the C-star IRC+10°216 (Cernicharo et al. 1986, Kahane et al. 1988). The other stellar data (circles) are for O-rich M-giants (Tsuji et al. 1994).

Fig. 16.— Fig. 7 of Lodders & Amari (2005, Chemie der Erde, 65, 93).

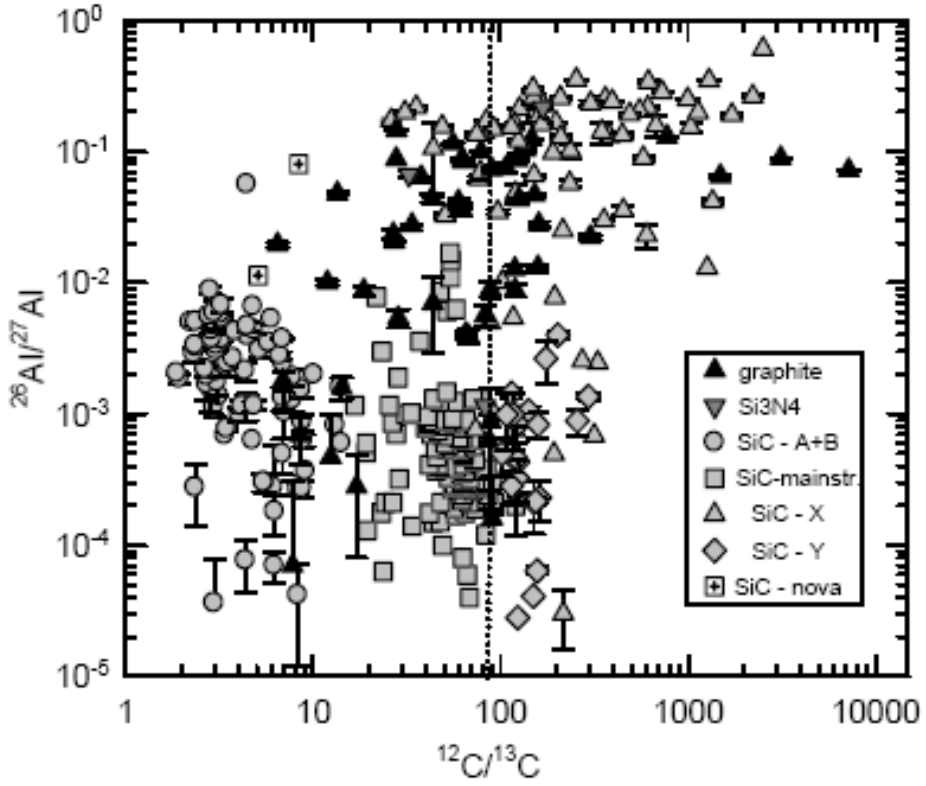

Fig. 8. Inferred $^{26}Al/^{27}Al$ ratios vs. $^{12}C/^{13}C$ ratios in SiC and low-density graphite grains. The SiC type X and graphite grains have the largest $^{26}Al/^{27}Al$. See text for data sources.

Fig. 17.— Fig. 8 of Lodders & Amari (2005, Chemie der Erde, 65, 93).

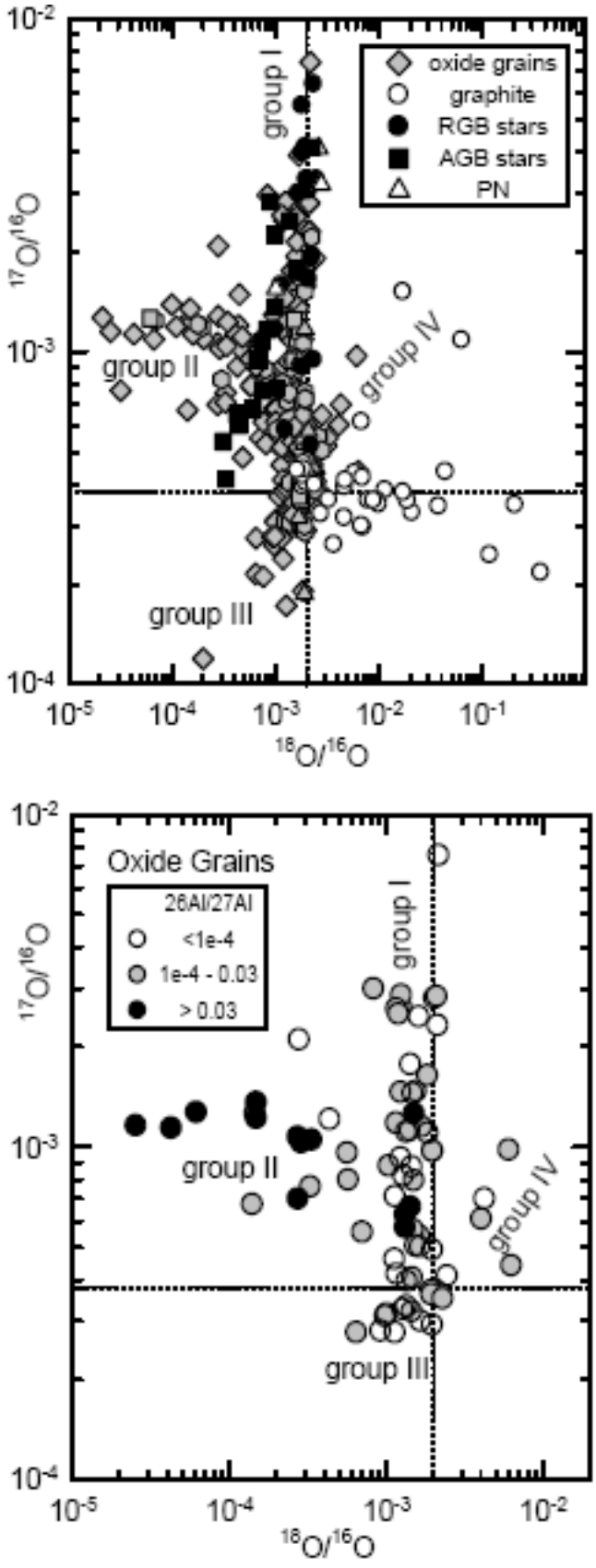

Fig. 18.— Figs. 14 and 15 of Lodders & Amari (2005, Chemie der Erde, 65, 93).

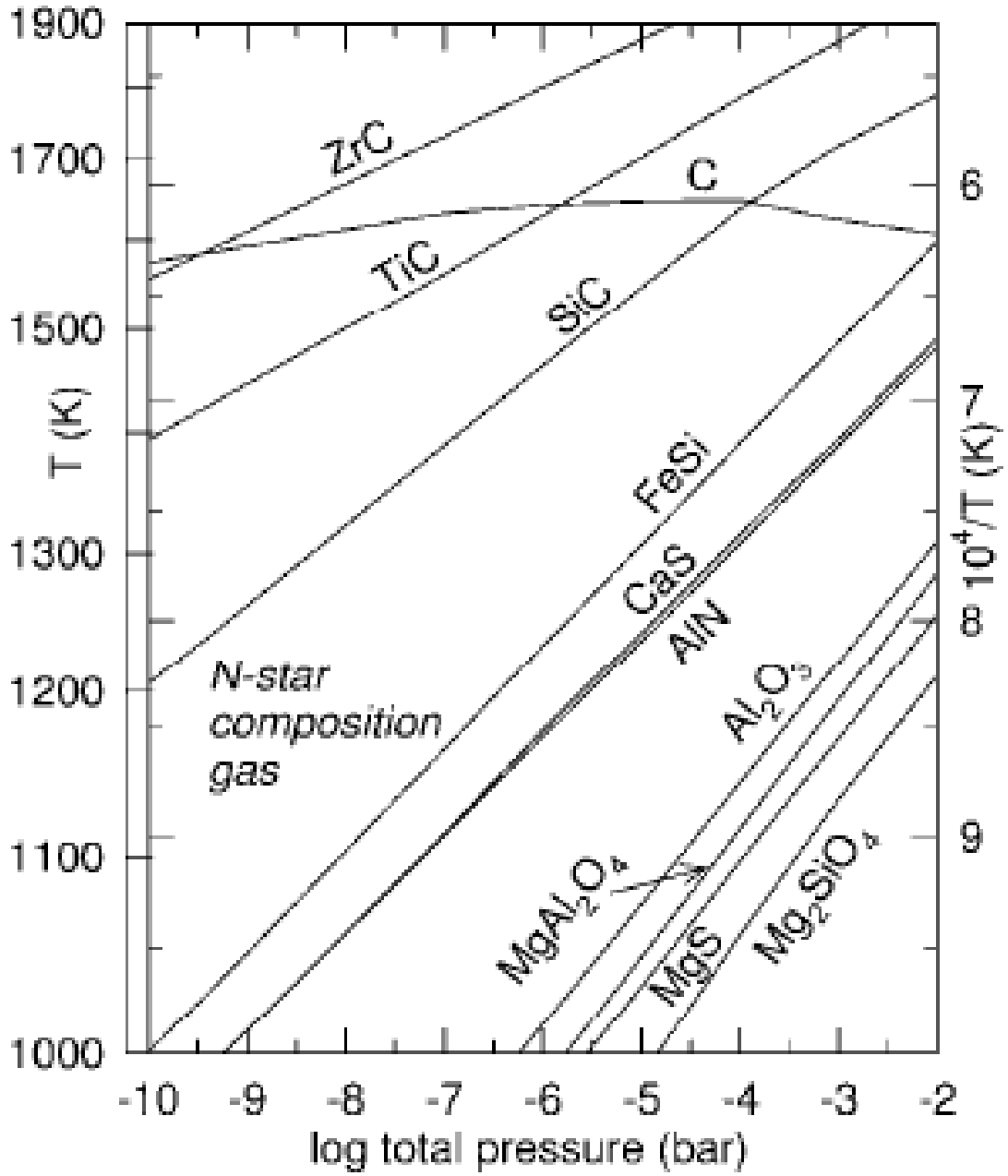

Fig. 21. Condensation temperatures as a function of total pressure at C/O = 1.1.

Fig. 19.— Fig. 21 of Lodders & Amari (2005, Chemie der Erde, 65, 93).

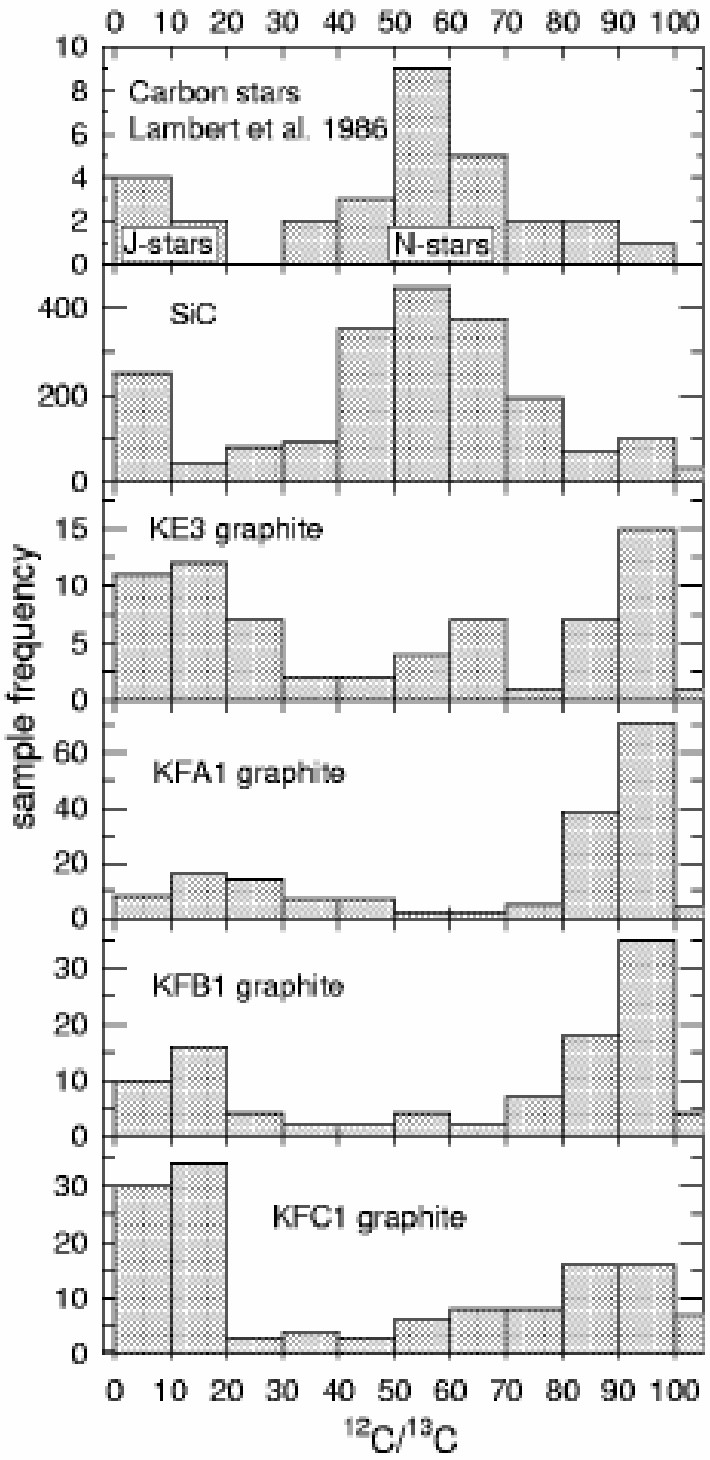

Fig. 22. Distribution of $^{12}C/^{13}C$ ratios in presolar SiC (Hoppe et al. 1994), presolar graphite (Hoppe et al. 1995, Travaglio et al. 1999, Amari, unpublished), and in C-stars (Lambert et al. 1986). Graphite and SiC data extend to $^{12}C/^{13}C$ of several thousand (Figs. 6, 8). Only the observed range for C-stars is covered here.

1.3. The Electromagnetic Spectrum – Gamma Rays

Gamma rays represent very energetic phenomena with energies $\sim$ 1 MeV. Such radiation is always non-thermal. For our purposes, the most common source of γ-rays is from decays, particularly those of common elements made in massive stars, which we can expect to eject lots of energy into the ISM, and so expect extended emission in the Galactic plane with higher flux from known OB associations.

A decay of a radioactive isotope may produce an emission line in the gamma-ray spectrum at the frequency corresponding to the appropriate energy.

The detections are difficult, as there are not a lot of such energetic photons emitted, and they must be observed above the Earth's atmosphere, or as showers of secondary particles at the surface of the Earth.

The most useful decays are that of unstable isotopes of relatively common elements, including ^{26}Al (mean lifetime $\sim 1 \times 10^6$ yr), ^{44}Ti (mean lifetime $\sim$65 yr) and ^{60}Fe (mean lifetime 1.5×10^6 yr). Because in some cases the mean lifetime of the unstable isotope to decay exceeds 10^6 yr, the material can diffuse reasonably far from its stellar source. The launch of the INTEGRAL telescope (the successor to the COMPTEL) has invigorated this field.

AGNs, blazars, and the transient, more powerful sources known as GRBs are superposed on this Galactic diffuse emission as point sources.

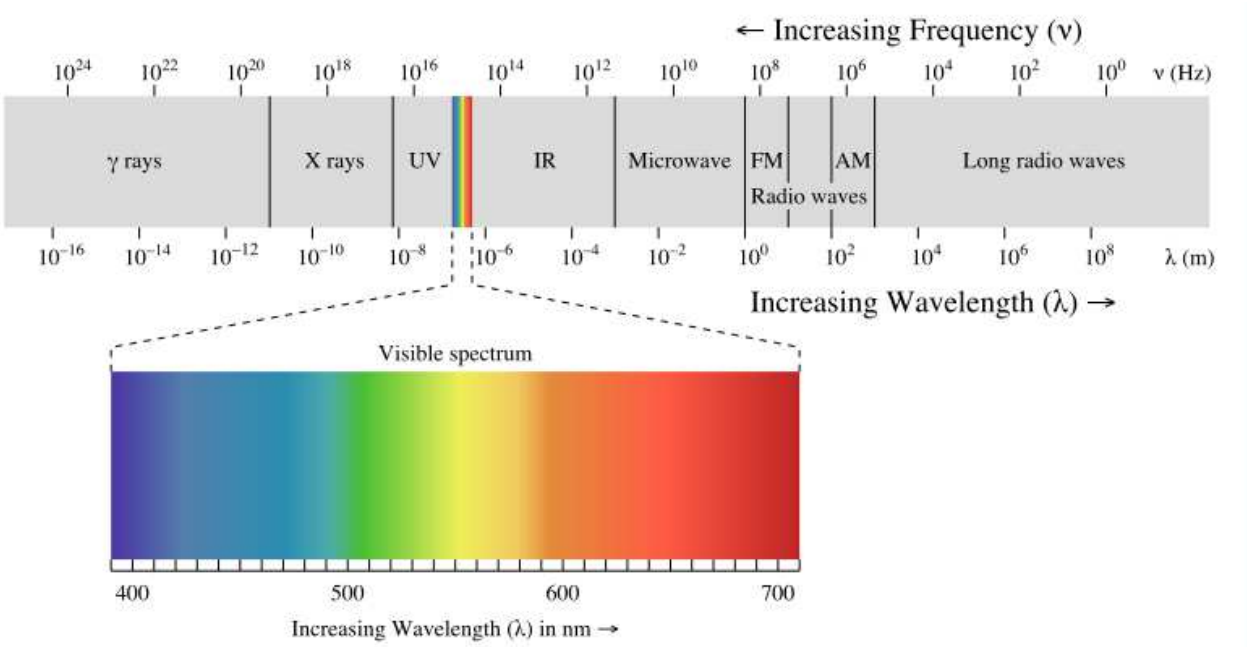

Fig. 21.— The regions of the electromagnetic spectrum. Recall that 912 Å is equivalent to 13.6 eV, so about 10^{-6} m is equivalent to a photon energy of 1 eV. (Source: Wikipedia Commons)

Measuring Cosmic Elements with Gamma-Ray Telescopes

Roland Diehl

Max Planck Institut für extraterrestrische Physik, D-85748 Garching, Germany (rod@mpe.mpg.de)

Abstract: Gamma-ray telescopes are capable of measuring radioactive trace isotopes from cosmic nucleosynthesis events. Such measurements address new isotope production rather directly for a few key isotopes such as ^{44}Ti, ^{26}Al, ^{60}Fe, and ^{56}Ni, as well as positrons from the β^+-decay variety. Experiments of the past decades have now established an astronomy with γ-ray lines, which is an important part of the study of nucleosynthesis environments in cosmic sources. For massive stars and supernovae, important constraints have been set: Co isotope decays in SN1987A directly demonstrated the synthesis of new isotopes in core-collapse supernovae, ^{44}Ti from the 340-year old Cas A supernova supports the concept of α-rich freeze-out, but results in interesting puzzles pursued by theoretical studies and future experiments. ^{26}Al and ^{60}Fe has been measured from superimposed nucleosynthesis within our Galaxy, and sets constraints on massive-star interior structure through its intensity ratio of $\sim$15%. The ^{26}Al γ-ray line is now seen to trace current star formation and even the kinematics of interstellar medium throughout the Galaxy. Positron annihilation emission from nucleosynthesis throughout the plane of our Galaxy appears to be mainly from ^{26}Al and other supernova radioactivity, but the striking brightness of the Galaxy's bulge region in positron annihilation gamma-rays presents a puzzle involving several astrophysics issues beyond nuclear astrophysics. This paper focuses mainly on a discussion of ^{26}Al and ^{60}Fe from massive star nucleosynthesis.

Fig. 22.— Abstract from a review conference proceeding by R. Diehl, *Measuring Cosmic Elements with Gamma-Ray Telescopes*, 2009, PASA.

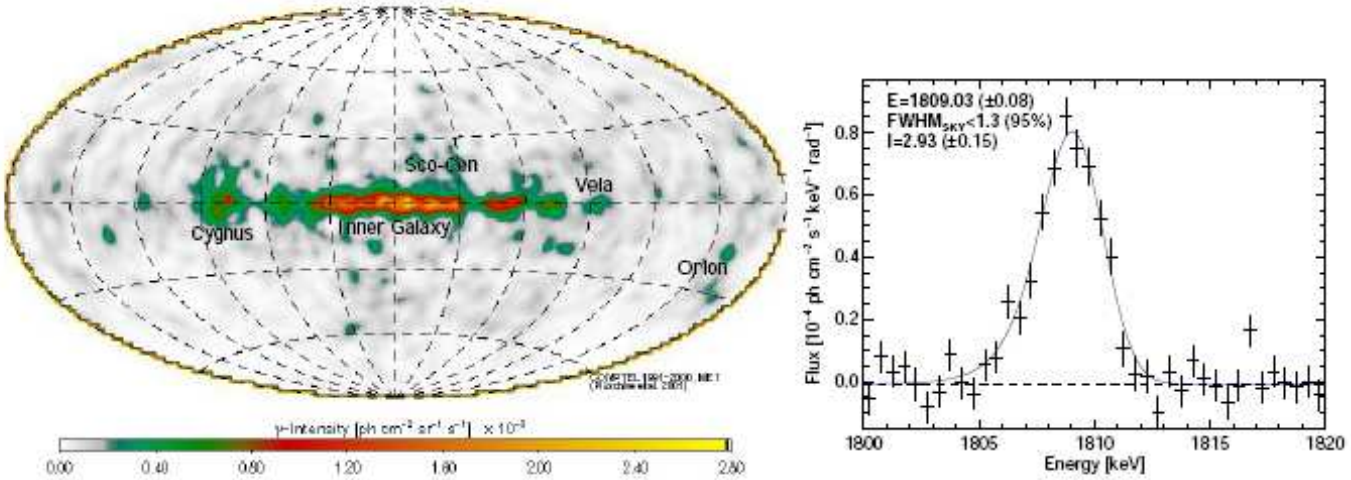

Figure 1: ^{26}Al radioactivity from the Galaxy, as seen by the Compton Observatory and INTEGRAL. (*Left:*): The ^{26}Al image from 9 years of sky survey with COMPTEL shows somewhat patchy emission along the plane of the Galaxy [29].(*Right:*): The ^{26}Al spectrum as measured by INTEGRAL/SPI shows the line to be rather narrow [30, 31]

Fig. 23.— Fig. 1 from Leising & Diehl, *Gamma-ray line studies of nucclei in the cosmos*, arXiv:0903.0772

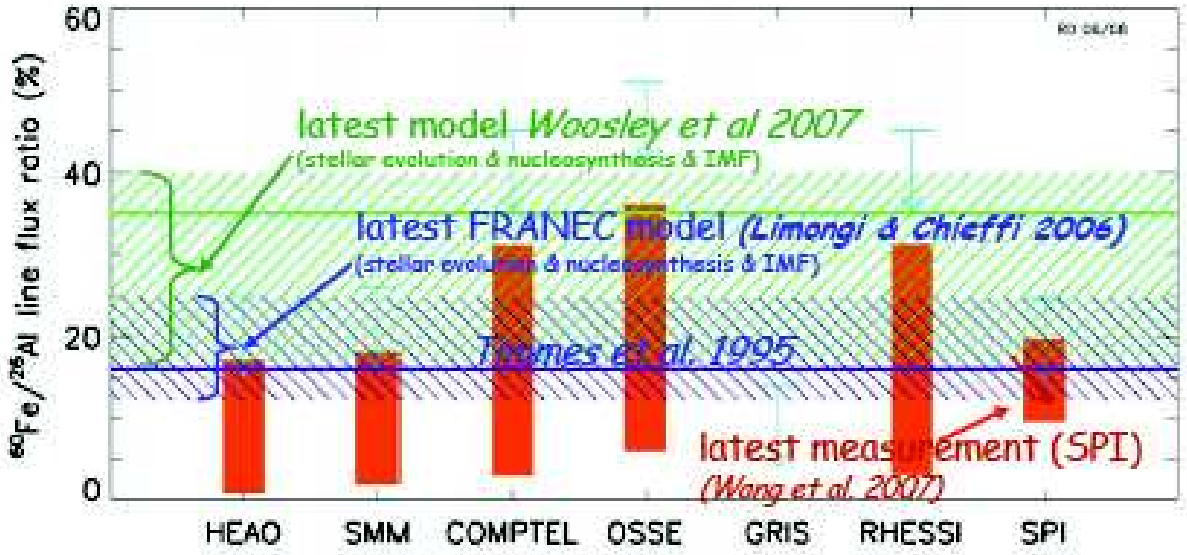

Figure 3: The ^{60}Fe/^{26}Al gamma-ray brightness ratio measurements from different gamma-ray experiments (19), as compared also to theoretical predictions (21; 22; 39) (see text).

Fig. 24.— Fig. 3 from a review conference proceeding by R. Diehl, *Measuring Cosmic Elements with Gamma-Ray Telescopes*, 2009, PASA.

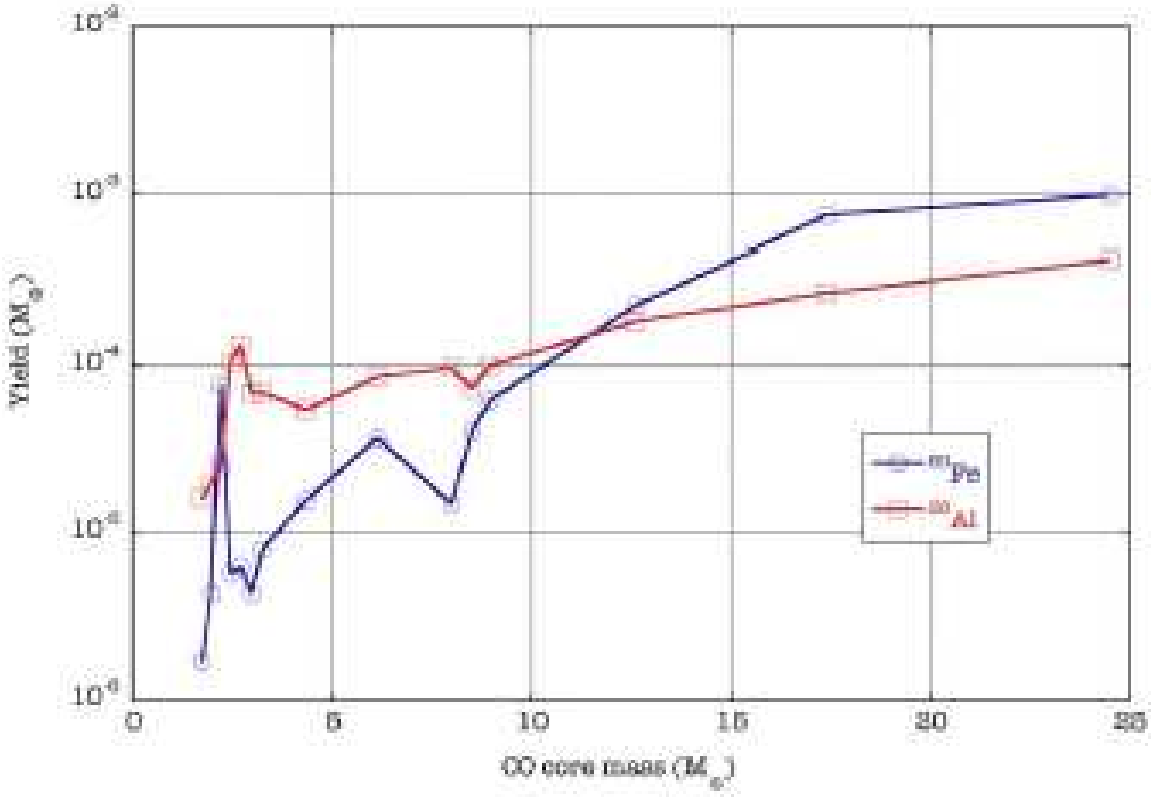

Fig. 1. Supernova yields of ^{26}Al and ^{60}Fe as a function of the CO core mass (from the models of LC06). These curves are used to associate the purely hydrostatic models of MMP05 with supernova yields.

Fig. 25.— Fig. 1 of Martin, Knodlseder, Meynet & Diehl, 2010, arXiv:1001.1522)

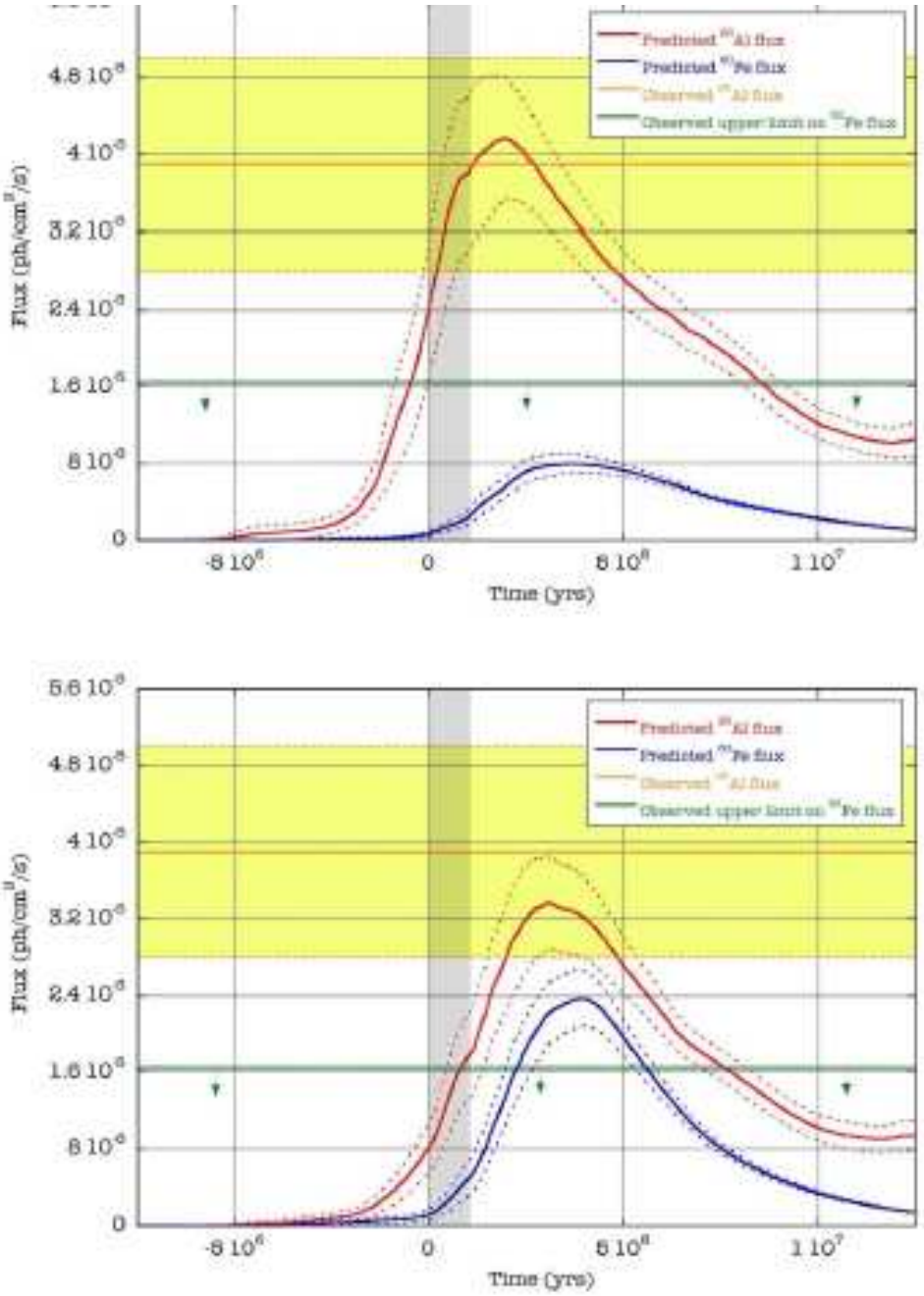

Fig. 5. Predicted versus observed decay fluxes, for Z=0.02 (solar) initial metallicity (top) and Z=0.01 initial metallicity (bottom). The red curve corresponds to the 1809 keV flux and the blue curve to the 1173/1332 keV flux. The dotted lines give the typical variance due to the finite IMF sampling. The orange band indicates the observed 1809 keV flux and the green line the upper limit on the 1173/1332 keV emission from the Cygnus complex. The vertical shaded area indicates our probable current position along the time axis (see text).

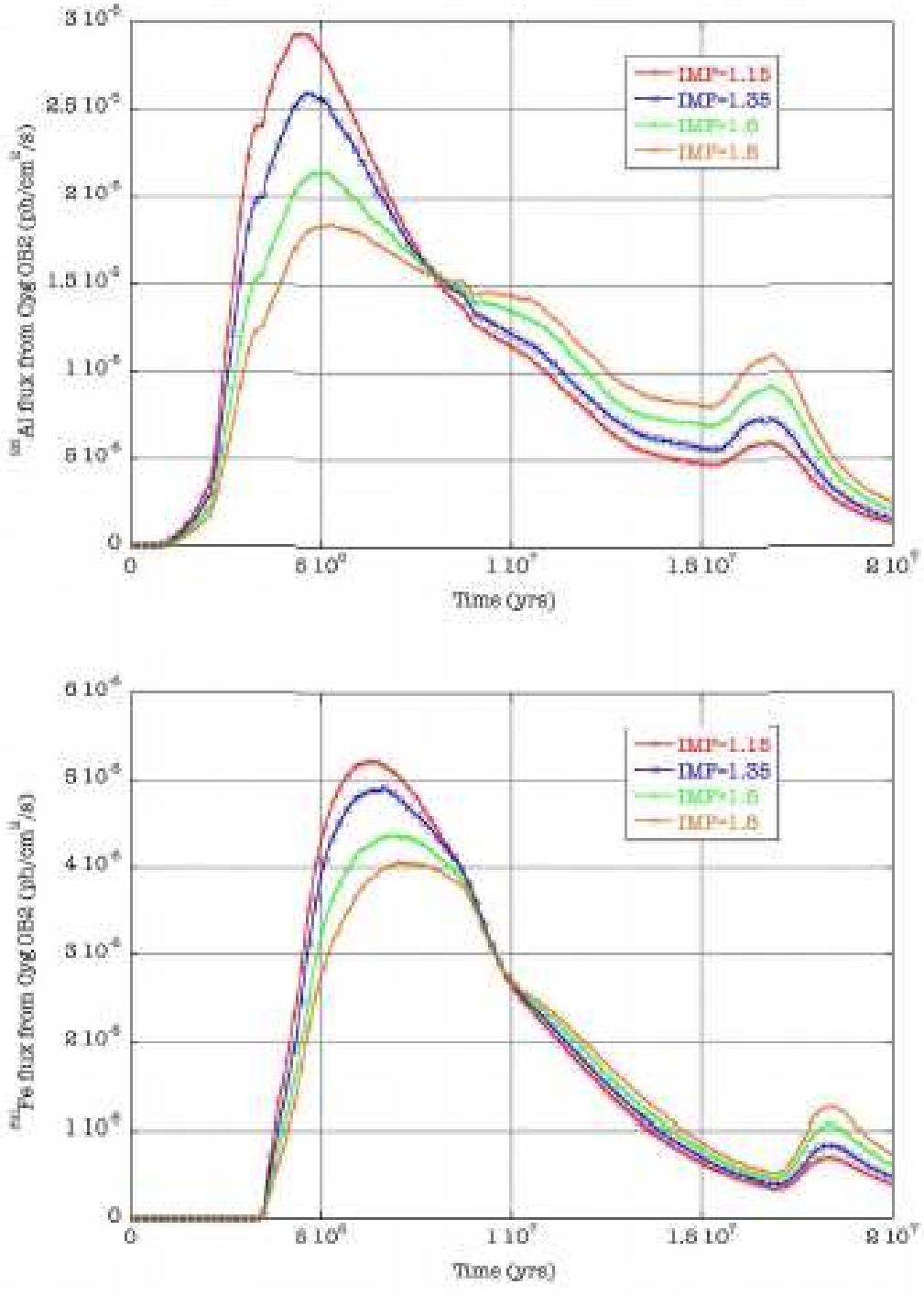

Fig. 6. Decay fluxes of ^{26}Al and ^{60}Fe from Cyg OB2 as a function of the IMF slope for an initial solar metallicity. In contrast to Fig. 5, the t=0 point does not mark the present day but instead the date of the coeval star formation.

Fig. 27.— Fig. 6 of Martin, Knodlseder, Meynet & Diehl, 2010, arXiv:1001.1522)

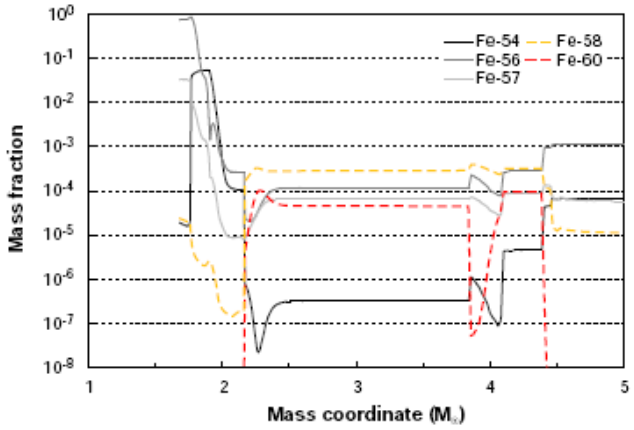

FIG. 3.— Post-supernova profile of Fe isotope abundances as a function of mass coordinate for a 19 $M_\odot$ cc-SN progenitor comp
rom zonal yields 25,000 s after core bounce (see Rauscher et al. 2002, for details). While ^{54}Fe, ^{56}Fe, and ^{57}Fe are produced as radioa
rogenitors in the internal regions of the cc-SN by nuclear statistical equilibrium, the neutron-rich isotopes ^{58}Fe and ^{60}Fe are proc
n more external regions by neutron-capture reactions on pre-existing Fe isotopes. [*See the electronic edition of the Journal for a*

Fig. 28.— The radial profile of various isotopes of Fe inside a $19M_\odot$ SNII progenitor. (Fig. 3 of Dauphas, Cook, Sacarabany et al, 2008, ApJ, 686, 560)

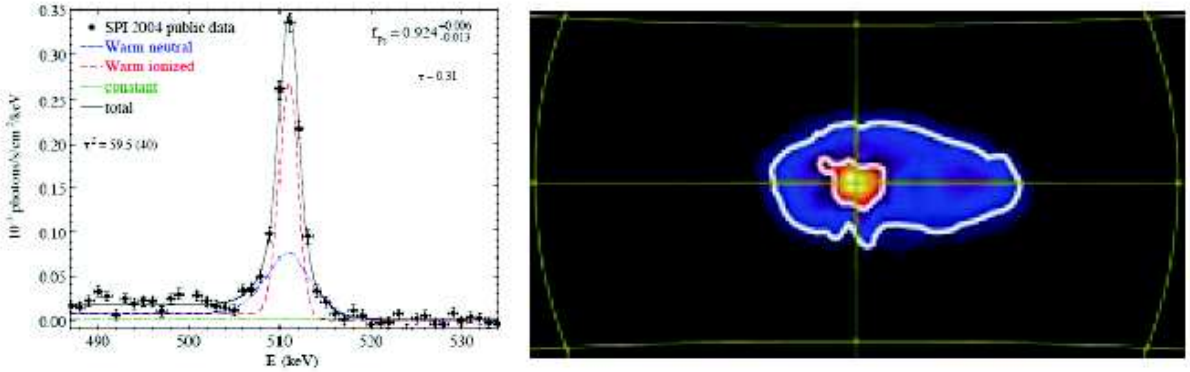

Figure 4: (*Left:*): The annihilation line spectrum as measured by INTEGRAL/SPI [50]. (*Right:*): The intensity of the annihilation line between galactic longitudes ±60°and latitudes ±30°, derived by an iterative maximum likelihood method (adapted from [51].)

Fig. 29.— Fig. 4 of Leising & Diehl, *Gamma-ray line studies of nucclei in the cosmos*, arXiv:0903.0772. Positron electron annihilation emission at 511 keV is much stronger in the central region of the Galaxy than in the disk, and is stronger than predicted. The positrons come from interactions of energetic CR protons with the ISM and subsequent decays of the resulting unstable products. The most likely decay channel for the positrons is $e^- + e^+ \rightarrow 2\gamma$, each with the rest mass energy of the electron or positron (511 keV).

1.4. Below Gamma-Ray Energies

X-ray photons from very hot gas (thermal source) such as might be found in a cluster of galaxies, as well as from various non-thermal sources such as SN, accreting black holes in the nuclei of galaxies, various types of energetic binaies, etc. Discrete line transitions are of very high energy and represent transitions within highly ionized atoms.

UV photons from hot stars, from soft X-ray sources. Discrete line transitions are from highly excited electronic states of ionized atoms, e.g. CIV at 1548 Å or the Lyman series of H. The Earth's atmosphere, even from a high mountain, is opaque in this wavelength regime, observations from satellites above the Earth's atmosphere are required.

Optical photons from continuum of normal stars, absorption features at a few eV correspond to transitions in the electronic configuration of many neutral and singly ionized atoms.

IR photons from cool stars, from dust in the ISM of the Milky Way and of other galaxies. The discrete line transtions are less than 1 eV, and usually arise from molecules. The Earth's atmosphere is more or less transparent, at least in a limited number of windows between strong terrestrial molecular absorption bands, but the thermal background problems are severe, and one does much better from (cold) space Note the success of Spitzer, a rather small telescope (diameter 0.85 m), whose sensitivity far exceeds that of a ground based 10 m telescope for broad band imaging, although not for photon-starved high dispersion spectroscopy in the near and mid-IR.

Microwave – CMB photons.

Radio - lowest rotational transitions in molecules, fine structure transition for H (21 cm line).

1.5. Cosmic Rays

Cosmic rays are fundamental particles or atomic nuclei that have been stripped of all their electrons that impact the Earth and can be detected from its surface. Most CRs are protons or He nuclei. They propagate through the ISM from sources (presumably SN) within the Galaxy, as well as, for the most energetic ones, from external galaxies. The normal model is to consider the Galaxy as a leaky box, then propagate the CR particles. A detailed propagation model can be found at http://galprop.stanford.edu/na_home.html. Interactions of cosmic rays with the ISM create secondary cosmic ray particles (see the section on Li, Be, and B), some of which are unstable. An example is ^{10}Be/^{9}Be. The isotopic ratios involving unstable nuclei are useful in constraining the timescale for propagation.

The ability to escape from the Galaxy, or to even penetrate the heliosphere and enter the Solar system itself, depends on the energy and nature of the CR and on the degree of Solar activity (i.e the strength of the Solar wind etc). The latter causes a solar modulation of the flux of low energy CRs as detected at the Earth.

The most useful things we want to know are the energy spectrum of the various elements and their isotopes that make up the cosmic rays. Also are the CRs isotropic ? Is there any sign of discrete sources ?

Traditionally, CR observatories were built on very high mountaintops, now there are big ground-based arrays of detectors of Cerenkov radiation (the Fly's Eye in Nevada, and more recently the Pierre Auger Observatory on the plains of Argentina). Ultra-high energy cosmic rays (energy $> 10^{19}$ eV) are very rare, and presumably largely extragalactic, from sources within $\sim$100 Mpc. They are detected via the extensive air showers initiated when such energetic particles impact the Earth's atmosphere.

Satellites such as the Advanced Composition Explorer (ACE, P.I. Ed Stone) also are

used to detect CR. ACE, launched in 1997, has been stationed at L1 for more than a decade. It can measure the mass, energy, and charge of each incident particle within specific limits. Galactic cosmic rays have a high enough energy in general to propagate through the Solar system. Interstellar charged plasma is kept out of the Solar system by the interplanetary magnetic field, but ISM neutral gas flows through the Solar system at a speed reflecting the velocity of the Sun with respect to the local standard of rest.

The ACE team has measured the flux of CRs of Li, Be, B and C as a function of energy, and used these to derive constraints on propagation models. The main purpose of ACE, however, is to study Solar activity and matter ejected from the Sun.

ACE data cannot be used directly to determine Solar surface abundances as the acceleration of particles from the Solar surface to the corona and beyond is not uniform for all particles, but is a function of mass, charge, and perhaps other parameters. Furthermore, the collecting area and mass discrimination of ACE is limited, and it cannot measure abundances for the rarest, heaviest elements.

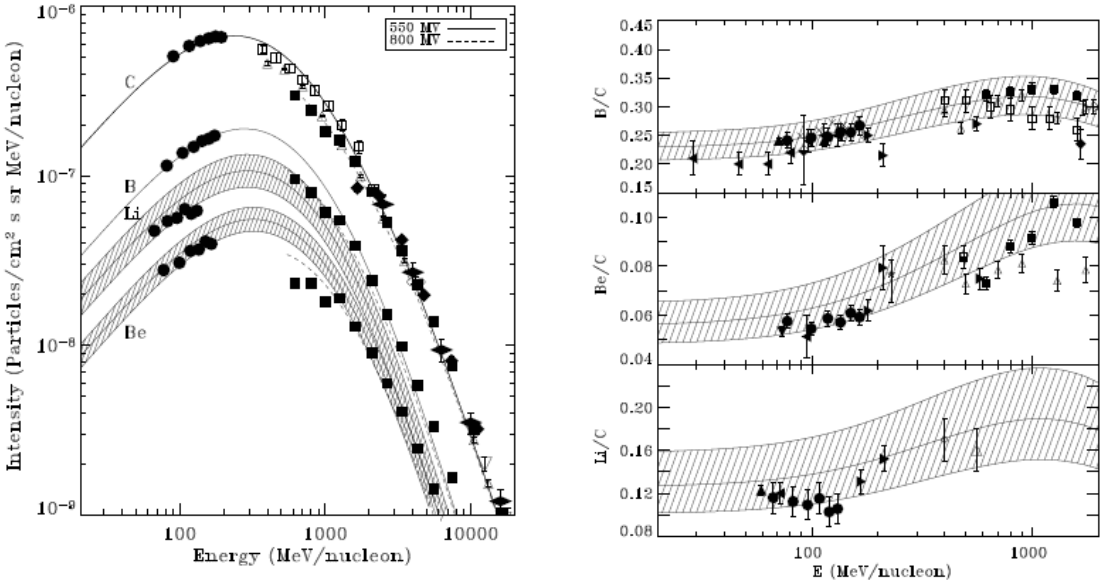

Fig. 1. [a] Intensities of C, B, Be, and Li shown for two levels of solar modulation ($\phi = 550$ (solid curve) and 800 MV (dashed curve)) corresponding to the epoch when the experimental data were taken, and [b] relative elemental abundances compared with previous observations. The experimental data is compared with the results of a propagation model GALPROP. See text for details. (Symbols refer to CRIS: ●, Maehl et al. 1977: □, Webber et al. 1972: △, Englemann et al. 1990: ■, Orth et al. 1978: ♦, Buffington et al. 1978: ◇, Simon et al. 1980: ◆, Buckley et al. 1994: ⬭, Chapel and Webber 1981: ▽, Lezniak et al. 1978: △, Muller et al. 1991: †, Dwyer et al. 1978: ▷, Webber et al. 1977: ▶, Garcia-Munoz et al. 1987: ◀, Duvernois et al. 1996: ∗, Mewaldt et al. 1981: ⧫, Wiedenbeck and Greiner 1980: ✚, Webber et al. 2002: ▼, Hagen et al. 1977: ★, Fisher et al. 1976: ⬓, Juliusson et al. 1974: +, Garcia-Munoz et al. 1977: ○, Connell et al. 2001: ×, Krombel et al. 1988: ◁, Lukasiak et al. 1999: ▲).

Fig. 30.— The energy distribution of cosmic rays of several light elements. The low energy end shape is affected by solar modulation. The high energy dropoff reflects the intrinsic spectrum. Fig. 1 of *Observations of Li, Be, and B isotopes and constraints on cosmic-ray propagation*, de Nolfo, Moskalenko, Binns et al (ACE team), 2006, Advances in Space Research, 38, 1558.

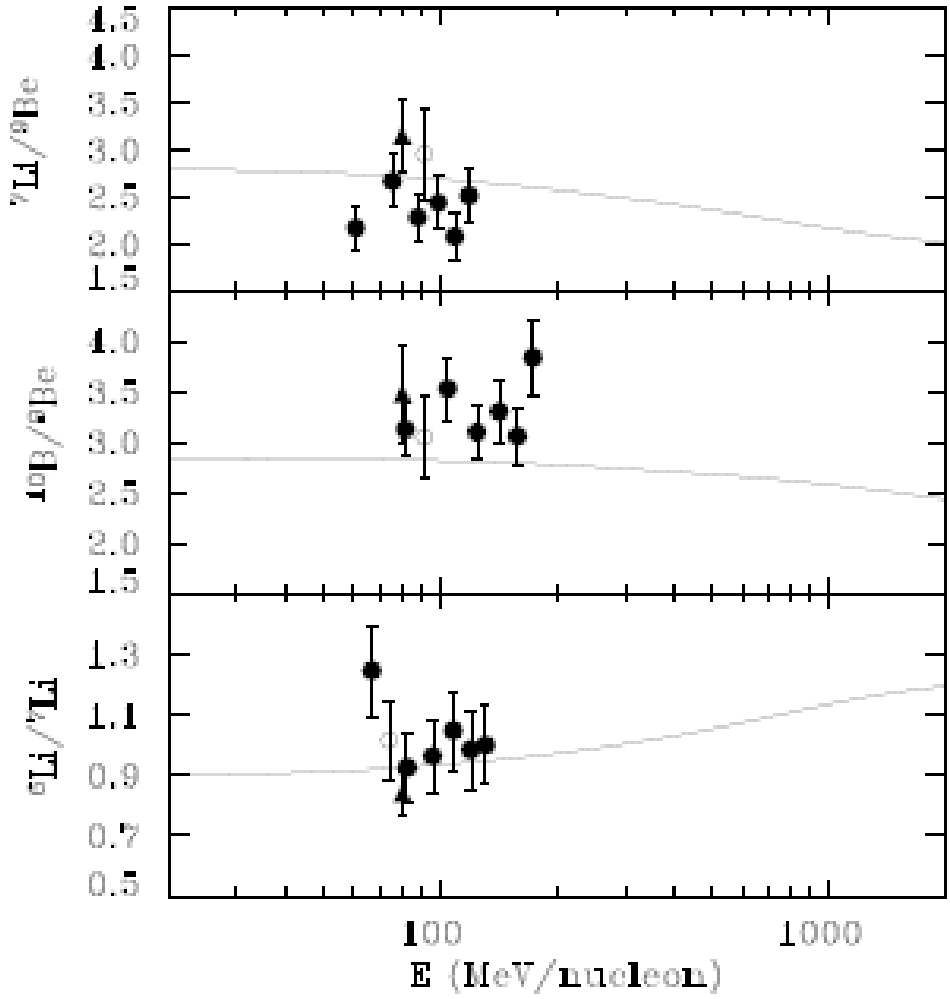

Fig. 2. Isotopic ratios of ^{6}Li/^{7}Li, ^{10}B/^{9}Be, and ^{7}Li/^{9}Be compared with previous data and with the predictions of GALPROP. (Data from CRIS: ●, Garcia-Munoz et al. 1977: ○, Lukasiak et al. 1999: ▲)

Fig. 31.— Fig. 2 of *Observations of Li, Be, and B isotopes and constraints on cosmic-ray propagation*, de Nolfo, Moskalenko, Binns et al (ACE team), 2006, Advances in Space Research, 38, 1558.

1.6. Stellar Matters

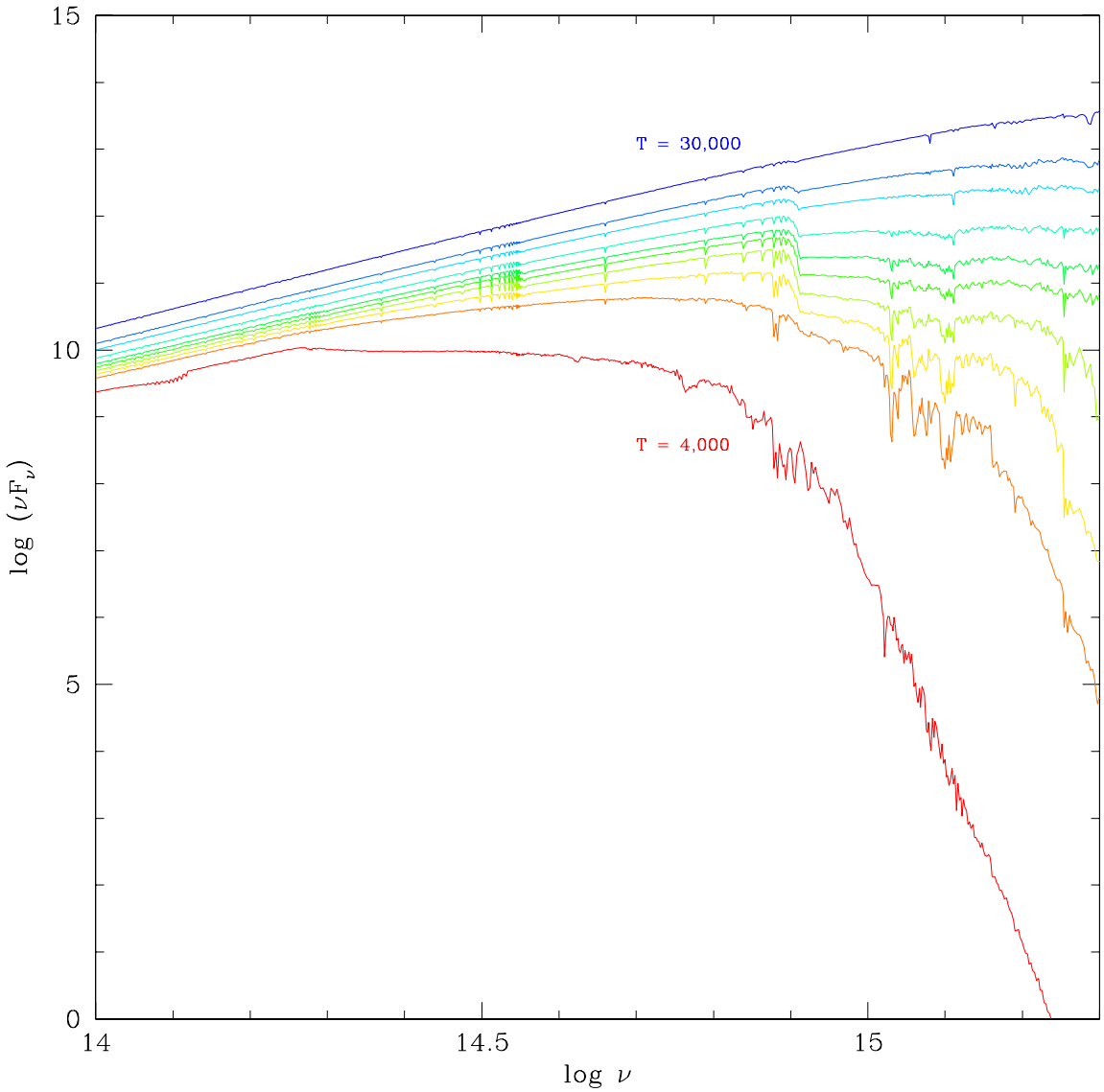

Fig. 32.— The spectral energy distribution of model stellar atmospheres of main sequence stars as a function of $T_{\rm eff}$. This figure is from R.L.Kurucz. Note that the range of $T_{\rm eff}$ observed for stars is from about 2000 K to 100,000 K.

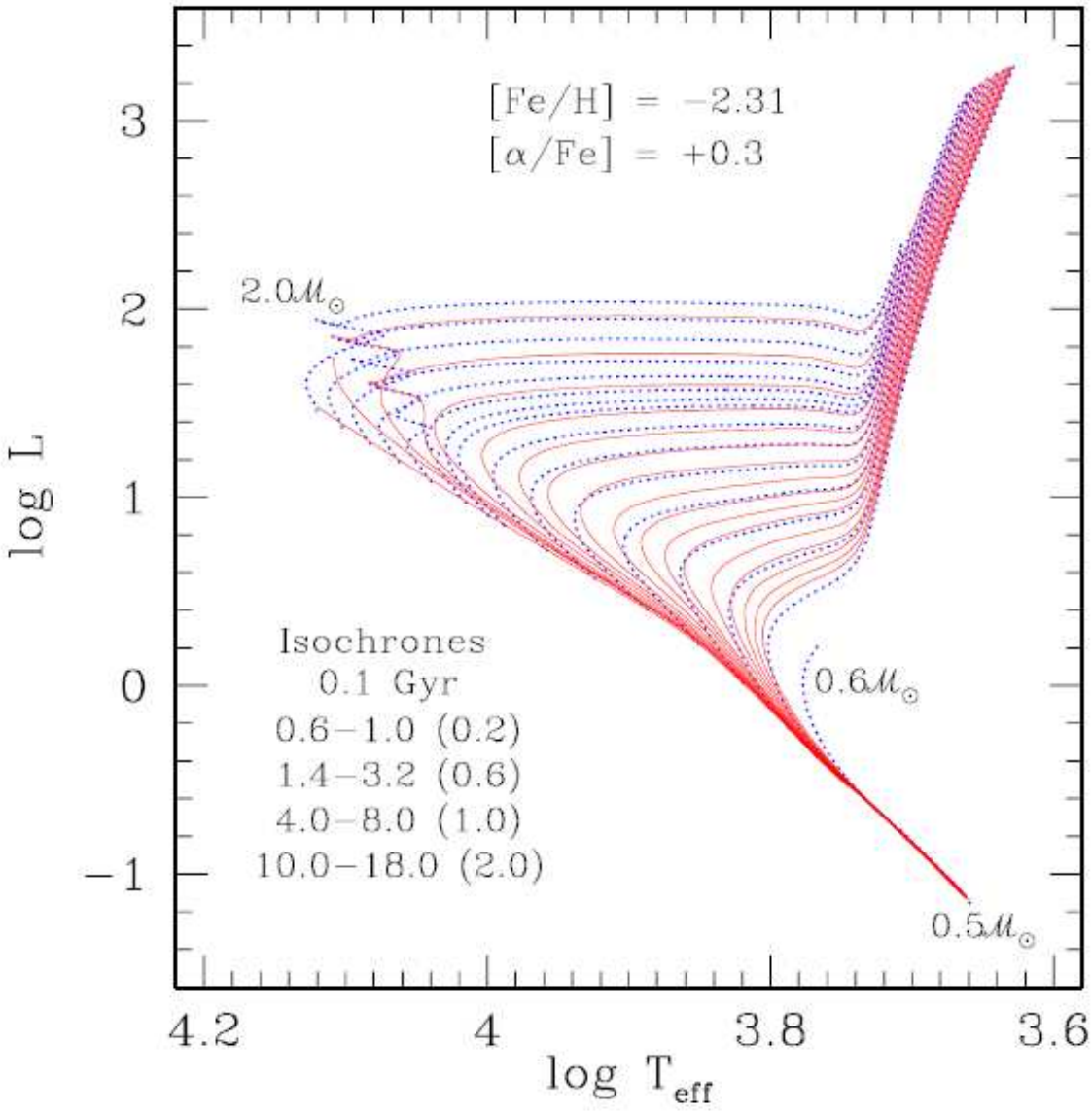

Fig. 9.— The complete grid of evolutionary tracks for the [Fe/H]= −2.31, [α/Fe] = +0.3 grid are plotted with the dotted blue lines. The tracks are spaced at 0.1$\mathcal{M}_\odot$ intervals with an additional track at 1.44$\mathcal{M}_\odot$, which is the transitional mass for the development of the blue hook. The isochrones, plotted as solid red lines, span the range of ages from 0.1 to 18.0 Gyr, as indicated.

Fig. 33.— Isochrones for stars of low metal content with ages from 0.1 to 18 Gyr. Note the overlap of all tracks for the lower main sequence where stars of low mass have not yet exhausted their H.

– 35 –

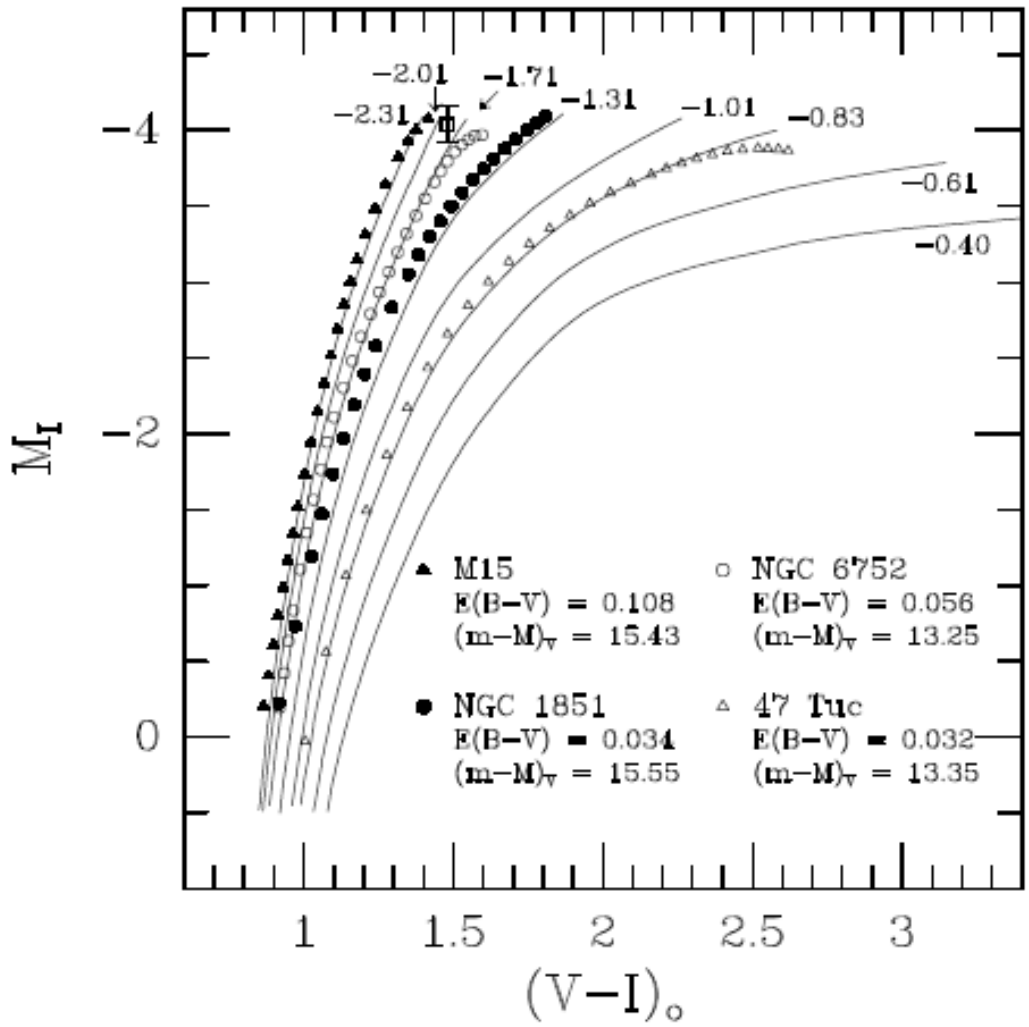

Fig. 13.— Overlay of the fiducial sequences derived by Da Costa & Armandroff (1990) for M15, NGC 6752, NGC 1851, and 47 Tucanae, on the assumption of the indicated reddenings and apparent distance moduli, onto the giant-branch segments of 13 Gyr isochrones for [Fe/H] values ranging from −2.31 to −0.40, assuming [α/Fe] = 0.3 in each case. Note that, as shown by VandenBerg (2000), turnoff ages close to 13 Gyr are consistent with the adopted $(m - M)_V$ values only for M 15 and NGC 6752: somewhat younger ages (≈ 11.5 Gyr) are obtained for NGC 1851 and 47 Tuc. The large open square, with error bars, gives the absolute I magnitude of the RGB tip stars in ω Centauri determined by Bellazzini et al. (2001); see the text.

Fig. 34.— Isochrones for stars of a range of metal content with a fixed age of 13 Gyr. Only the region of the red giant branch is shown. Fiducial lines for 4 well studied Galactic globular clusters are shown. Overlapping theory and data requires specifying the distance and the interstellar reddening of each cluster.

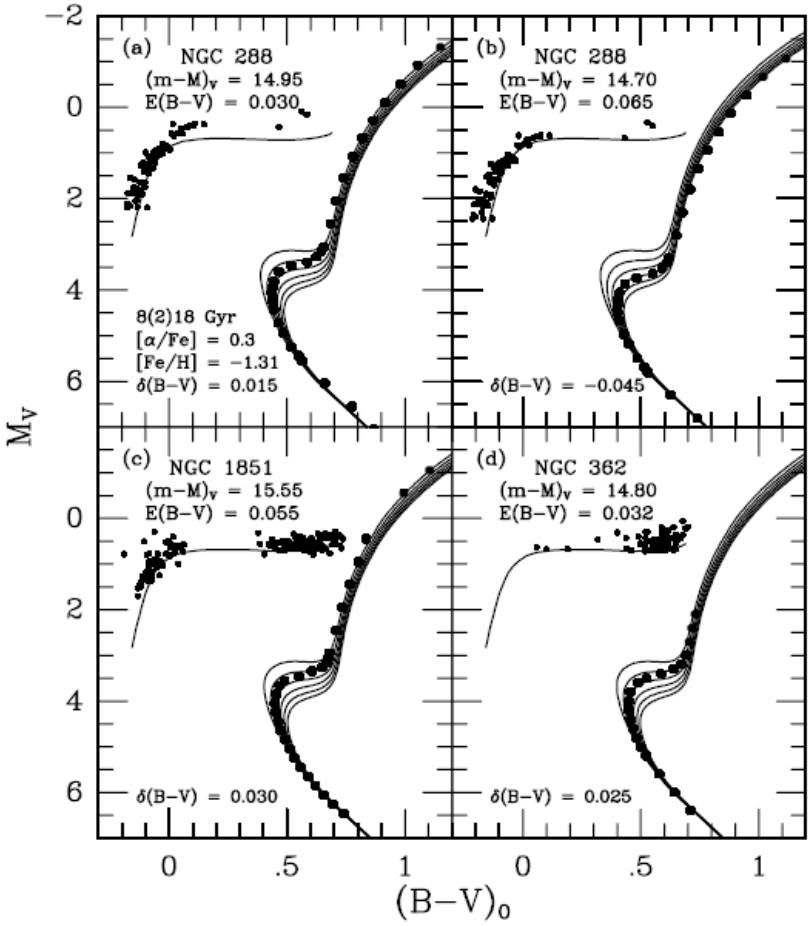

FIG. 28.—Panels (*a*) and (*b*) illustrate two of many possible fits of our ZAHB and isochrones for the indicated parameters to the NGC 288 CMD. The fiducial for the main sequence and giant stars is as defined in Fig. 23: the HB photometry is from Bergbusch (1993), but corrected by +0.01 mag in $B-V$ and −0.0635 mag in V to place those data on the system of Bolte (1992) photometry. Panels (*c*) and (*d*) show how well the same models match the NGC 1851 (Walker 1992b) and NGC 362 (VBS, Harris 1982) CMDs, respectively. The adopted reddening for the latter is from the SFD maps, while that for the former is based on the fit of the ZAHB to the blue HB stars (see the text for some discussion of this point).

Fig. 35.— Isochrones for stars of a range of metal content with a fixed age (13 Gyr ?). Fiducial lines for 4 well studied Galactic globular clusters are shown including the lower main sequence and the RGB. Individual horizontal branch stars are shown as well.

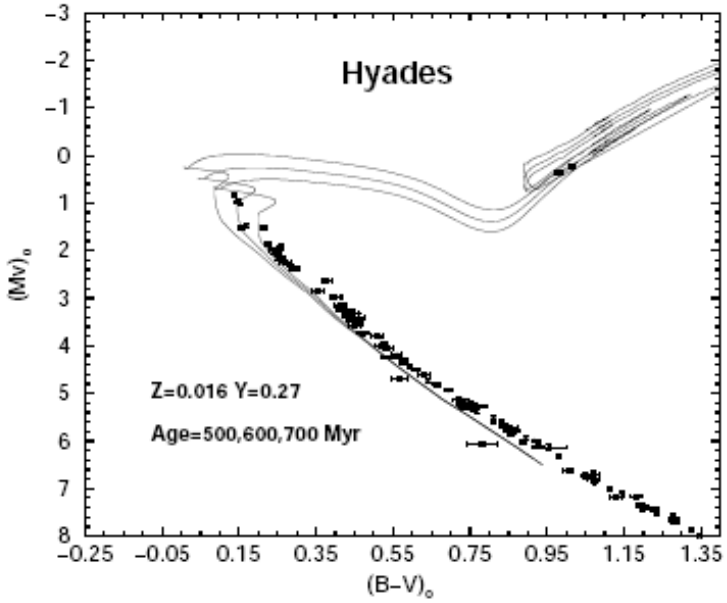

FIG. 3. The CMD for the Hyades, using the parallax values from Madsen et al. (2002). Visual, spectroscopical and suspected binaries are excluded, see also Madsen et al. (2000). Error bars indicate observational errors as given by Madsen et al. (2002) for the parallax and by the Hipparcos catalog (at the node http://astro.estec.esa.nl/Hipparcos/HIPcataloguesearch.html) for the colors. Observational data are compared with present theoretical isochrones for Z=0.016 Y=0.27 α=1.9. Color transformations and bolometric corrections from Castelli (1999).

Fig. 36.— Match of observations and theoretical isochrones for stars in the nearby Hyades cluster, believed to have an age of about 400 Myr. Note the presence of stars significantly more luminous (i.e. massive) than the Sun still on the main sequence.

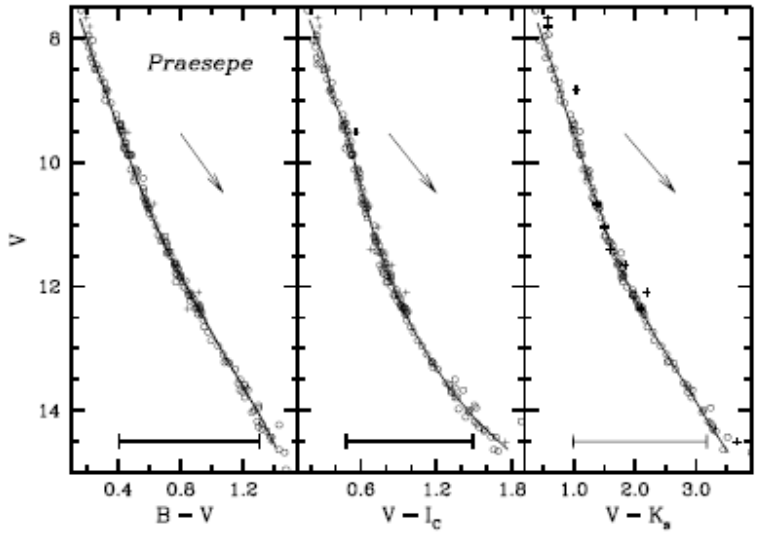

FIG. 6.— CMDs of Praesepe, after excluding known binaries and stars with low membership probability. Plusses are photometrically rejected data points from the filtering algorithm, and open points are those remaining. The solid lines are empirically calibrated isochrones with spectroscopic metallicity (Table 9), which were adjusted for the reddening with the literature value (Table 9). Fitting ranges are shown as horizontal bars. The arrow denotes the direction of reddening vectors.

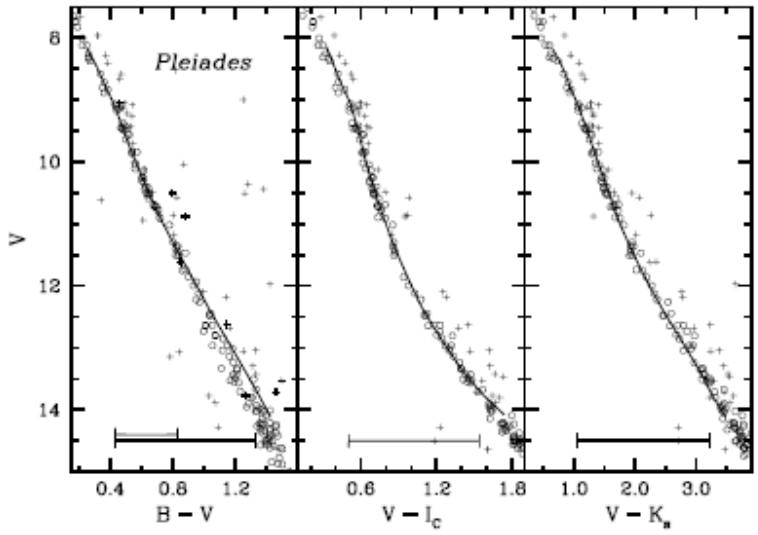

FIG. 7.— Same as Fig. 6, but for the Pleiades. As discussed by Stauffer et al. (2003), the Pleiades K dwarfs are bluer than the given isochrone in $(B-V, V)$, but not in the other two CMDs (see text). The distance modulus in $(B-V, V)$ was derived at $0.4 \leq (B-V)_0 \leq 0.8$ as shown by the shorter horizontal bar.

Fig. 37.— Match of observations and theoretical isochrones for stars on the lower main sequence of the nearby young clusters Pleides and Praesepe. Note the very tight locus of the low mass cluster members, with a few obvious interloper non-member field stars.

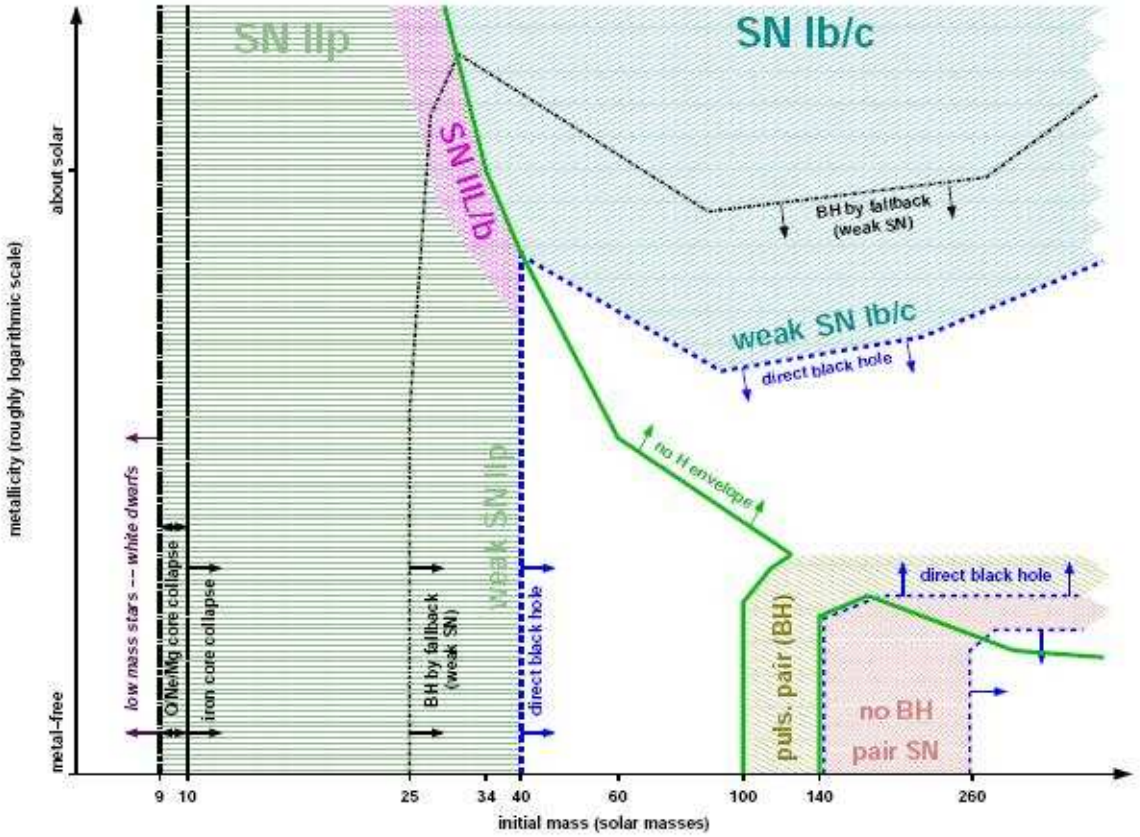

Fig. 2.— Supernovae types of non-rotating massive single stars as a function of initial metallicity and initial mass. The lines have the same meaning as in Fig. 1. *Green horizontal hatching* indicates the domain where Type IIp supernovae occur. At the high-mass end of the regime they may be weak and observationally faint due to fallback of ^{56}Ni. These weak SN Type IIp should preferentially occur at low metallicity. At the upper right edge of the SN Type II regime, close to the *green line* of loss of the hydrogen envelope, Type IIL/b supernovae that have a hydrogen envelope of $\lesssim 2\,M_\odot$ are made (*purple cross hatching*). In the upper right quarter of the figure, above both the lines of hydrogen envelope loss and direct black hole formation, Type Ib/c supernovae occur; in the lower part of their regime (middle of the right half of the figure) they may be weak and observationally faint due to fallback of ^{56}Ni, similar to the weak Type IIp SNe. In the direct black hole regime no "normal" (non-jet powered) supernovae occur since no SN shock is launched. An exception are pulsational pair-instability supernovae (lower right corner; *brown diagonal hatching*) that launch their ejection before the core collapses. Below and to the right of this we find the (non-pulsational) pair-instability supernovae (*red cross hatching*), making no remnant, and finally another domain where black hole are formed promptly at the lowest metallicities and highest masses (*while*) where nor SNe are made. White dwarfs also do not make supernovae (*white strip* at the very left).

.

Fig. 38.— The mode of stellar death for single stars as a function of initial stellar mass. Low mass stars become white dwarfs, while stars with $M \gtrsim 8_\odot$ become SN of various types. Fig. after Heger & Woosley.

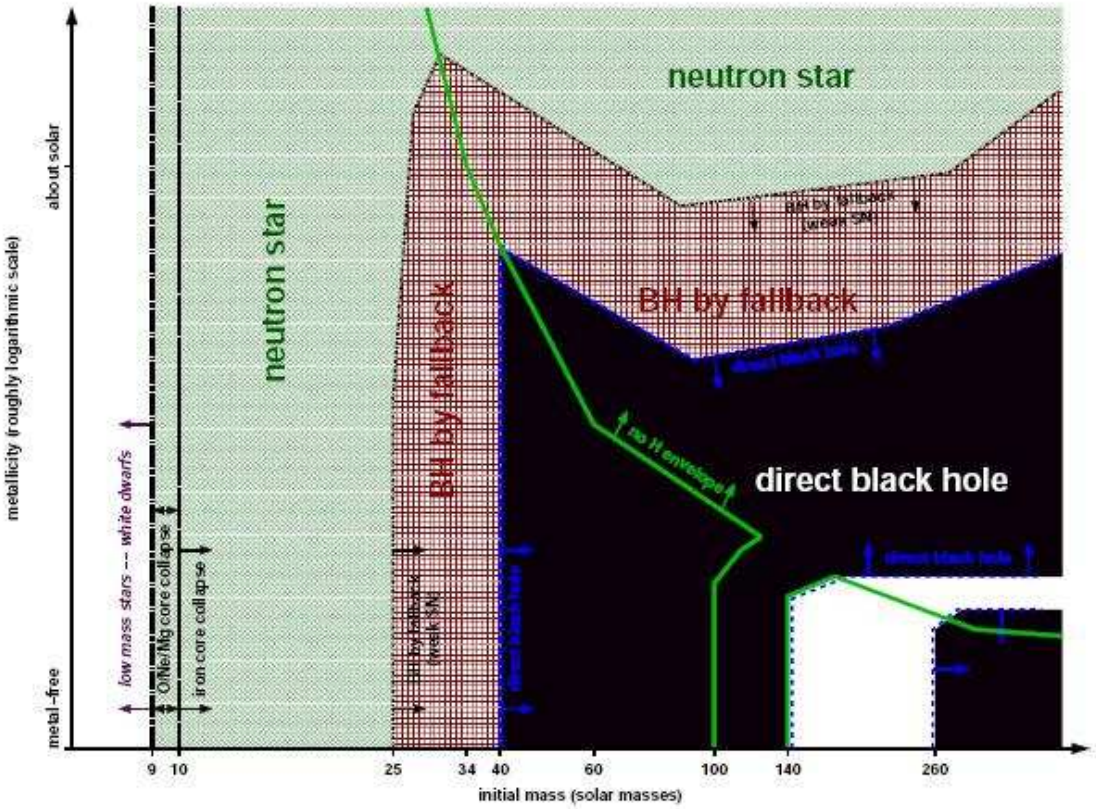

Fig. 1.— Remnants of massive single stars as a function of initial metallicity (*y-axis*; qualitatively) and initial mass (*x-axis*). The *thick green line* separates the regimes where the stars keep their hydrogen envelope (left and lower right) from those where the hydrogen envelope is lost (upper right and small strip at the bottom between 100 and 140 $M_\odot$). The *dashed blue line* indicates the border of the regime of direct black hole formation (*black*). This domain is interrupted by a strip of pair-instability supernovae that leave no remnant (*white*). Outside the direct black hole regime, at lower mass and higher metallicity, follows the regime of BH formation by fallback (*red cross hatching* and bordered by a *black dash-dotted line*). Outside of this, *green cross hatching* indicates the formation of neutron stars. The lowest-mass neutron stars may be made by O/Ne/Mg core collapse instead of iron core collapse (*vertical dash-dotted lines* at the left). At even lower mass, the cores do not collapse and only white dwarfs are made (*white strip* at the very left).

Fig. 39.— The remnant at the end stage of the evolution of a single star is shown as a function of mass and metal content. Possibilities include white dwarfs, neutron stars, black holes, no remnent left at all, etc. Fig. after Heger & Woosley.

2. Topics for student discussion

1. The families of pre-solar grains and how to distinguish between an SN origin and a cool star wind origin.

2. Predicting the γ-ray flux from a young cluster of stars of a specified mass, age, and metallicity at a specified distance from us in the Milky Way.

3. Solar abundances from the solar wind vs those of the photosphere.

4. Current views of the disagreement between predictions of modes of helioseismology and the latest Solar abundances.